Deglacial history of the West Antarctic Ice Sheet in the western Amundsen Sea Embayment

James A. Smith[1*], Claus-Dieter Hillenbrand[1], Gerhard Kuhn[2], Robert D. Larter[1], Alastair G.C. Graham[1], Werner Ehrmann[3], Steven G. Moreton[4], Matthias Forwick[5].

[1]*British Antarctic Survey, High Cross, Madingley Road, Cambridge, CB3 0ET, UK.*

[2]*Alfred Wegener Institute for Polar and Marine Research, P.O. Box 120161, D-27515 Bremerhaven, Germany*

[3]*Institute for Geophysics and Geology, University of Leipzig, Talstrasse 35, D-04103 Leipzig, Germany.*

[4]*NERC Radiocarbon Facility (Environment), East Kilbride, UK*

[5]*University of Tromsø, Department of Geology, N-9037 Tromsø, Norway*

*Corresponding author:

Tel.: +44 1223 221229; fax: +44 1223 221646

E-mail address: jaas@bas.ac.uk (James A. Smith)

Abstract

The Amundsen Sea Embayment (ASE) drains approximately 35% of the West Antarctic Ice Sheet (WAIS) and is one of the most rapidly changing parts of the cryosphere. In order to predict future ice-sheet behaviour, modellers require long-term records of ice-sheet melting to constrain and build confidence in their simulations. Here, we present detailed marine geological and radiocarbon data along three palaeo-ice stream tributary troughs in the western ASE to establish vital information on the timing of deglaciation of the WAIS since the Last Glacial Maximum (LGM). We have undertaken multi-proxy analyses of the cores (core description, shear strength, x-radiographs, magnetic susceptibility, wet bulk density, total organic carbon/nitrogen, carbonate content and clay mineral analyses) in order to: (1) characterise the sedimentological facies and depositional environments; and (2) identify the horizon(s) in each core that would yield the most reliable age for deglaciation. In accordance with previous studies we identify three key facies, which offer the most reliable stratigraphies for dating deglaciation by recording the transition from a grounded ice sheet to open marine environments. These facies are: i) subglacial, ii) proximal grounding-line, and iii) seasonal open-marine. In addition, we incorporate ages from other facies (e.g., glaciomarine diamictons deposited at some distance from the grounding line, such as glaciogenic debris flows and iceberg rafted diamictons and turbates) into our deglacial model. In total, we have dated 78 samples (mainly the acid insoluble organic (AIO) fraction, but also calcareous foraminifers), which include 63 downcore and 15 surface samples. Through careful sample selection prior to dating, we have established a robust deglacial chronology for this sector of the WAIS. Our data show that deglaciation of the western ASE was probably underway as early as

22,351 calibrated years before present (cal yr BP), reaching the mid-shelf by 13,837 cal yr BP and the inner shelf to within c.10-12 km of the present ice shelf front between 12,618 and 10,072 cal yr BP. The deglacial steps in the western ASE broadly coincide with the rapid rises in sea-level associated with global meltwater pulses 1a and 1b, although given the potential dating uncertainty, additional, more precise ages are required before these findings can be fully substantiated. Finally, we show that the rate of ice-sheet retreat increased across the deep (up to1,600 m) basins of the inner shelf, highlighting the importance of reverse slope and pinning points in accelerated phases of deglaciation.

Keywords: *West Antarctic Ice Sheet (WAIS), Last Glacial Maximum (LGM), Amundsen Sea, dating, deglaciation, reverse slope*.

1. Introduction

One of the largest uncertainties in the Intergovernmental Panel on Climate Change's projection of future sea level is the uncertain behaviour of the largely marine-based West Antarctic Ice Sheet (WAIS). The Amundsen Sea Embayment (ASE) drains approximately 35% of the WAIS and is one of the most rapidly changing parts of the cryosphere. Over the last two decades surface elevations of glaciers in the ASE (e.g., Pine Island and Thwaites) have decreased by 3.5 to 5.5 ma-1 (Shepherd et al. 2004; Scott et al., 2009) leading some to suggest that complete collapse of the ice in these catchments is possible on human time-scales (Katz and Worster, 2010). If this were to happen, it would raise global eustatic sea level by an estimated 1.2-1.5 m (Vaughan, 2008).

Ice sheets have long reaction timescales due to the complex interplay between isostasy, thermo-mechanical coupling and advection of ice with different rheological properties in the basal shear layers (Bentley, 2009). Thus, in the context of recent rapid thinning and grounding line retreat of glaciers in the Amundsen Sea, it is still unclear whether these changes are: (1) a rapid phase of a long-term, stepwise retreat that began with warming and/or sea-level rise shortly after the LGM; or (2) a response to a recent atmospheric/oceanic forcing. To determine which of these scenarios is correct accurate reconstructions of the post-LGM deglacial history are necessary. Accurate information on past ice sheet configurations and deglacial 'trajectories' will help improve our understanding of contemporary ice sheet behaviour and thus constrain numerical ice sheet models which aim to predict future sea-level change.

In this paper we establish a detailed deglacial history for the western ASE, encompassing the Dotson and Getz Ice shelves (Fig. 1), using direct evidence on the timing of retreat from sedimentological and radiocarbon data, analysed in 31 sediment cores. In addition, we compare the timing of post-LGM ice-sheet retreat in this region to the regional picture of deglaciation along the Pacific margin of the WAIS, discuss the style and rate of deglaciation, and comment on whether ice from the western ASE contributed to global meltwater pulses (mwps).

2. Study area and previous work

The Getz Ice Shelf is over 480 km long and 32 to 96 km wide, bordering the Hobbs and Bakutis Coasts of Marie Byrd Land between McDonald Heights (west of our map) and Martin Peninsula (Fig. 1). The Dotson Ice Shelf is c. 48 km wide between Martin and Bear Peninsulas on the coast of Marie Byrd Land. Both ice shelves have thinned dramatically during the past two decades with recorded elevation changes of -36 ± 2 cm year^{-1} and -17 ± 6 cm year^{-1} from 1992 to 2001 (Shepherd et al. 2004). In addition the Kohler Glacier, buttressed by the Dotson Ice Shelf, is thinning rapidly and its flow speed accelerated by 10-50% between 1996 and 2005 (Rignot, 2006). These rates, particularly those of the Dotson Ice Shelf, are comparable to the thinning and flow acceleration of Pine Island Glacier (PIG), and thus suggest common forcing(s). Rapid ice-shelf thinning in the ASE has been linked to basal melting by warm Circumpolar Deep Water (CDW) which is thought to have resulted in a reduction in buttressing force, ice flow acceleration, dynamic thinning and grounding line (GL) retreat (Shepherd et al., 2004; Payne et al., 2004; 2007; Walker et al., 2007; Thoma et al., 2008; Jenkins et al., 2010).

In the western ASE, three c. 1,000-1,600 m deep tributary troughs extend seawards from the modern ice shelf fronts, eventually merging into a single cross shelf trough, approximately 65 km wide and 600 m deep (Fig. 1; western ASE palaeo ice stream trough) (Larter et al., 2007, 2009; Nitsche et al., 2007; Graham et al., 2009). The mid-shelf trough then shallows seaward, but continues NW to the shelf edge where its axis, between 118–119° W, is still deeper than 500 m (Fig. 1). The easternmost tributary trough extends from beneath the Dotson Ice Shelf and the other two extend from below parts of the Getz Ice Shelf either side of Wright Island. Hereafter we refer to them as the Dotson, Getz A and Getz B tributary troughs, in order from east to west (Fig. 1). Elongated subglacial bedforms imaged close to the modern ice fronts in the Dotson and Getz A tributary troughs develop into mega-scale glacial lineations (MSGL) further offshore. The tributary troughs then merge into the main Dotson-Getz Trough (Larter et al., 2009; Graham et al., 2009). Similarly elongated bedforms, within 40 km of the Getz B ice front, suggest that streaming flow also occurred at least in the NE part of that tributary trough. The pattern of bedforms within the troughs indicates flow convergence northwards and represents a major palaeo-drainage route of the WAIS during the LGM, with grounded ice probably extending to the continental shelf edge (Larter et al., 2009; Graham et al., 2009).

The timing of deglaciation in the ASE remains poorly constrained. Three cores recovered from the inner shelf of Wrigley Gulf, to the west of Siple Island (Getz D using our terminology; Fig. 1) indicate the onset of open-marine sedimentation occurred sometime between 14,750 and 15,215 cal yr BP (13,873 and 14,194 ^{14}C yr BP; uncorrected age; Anderson et al., 2002). More recently, Hillenbrand et al. (2010a) studied five sediment cores (VC424, 425, PS69/273, PS69/274, PS69/275) collected in the western ASE. The cores recovered an almost pure diatomaceous ooze unit directly above the grounding-line proximal facies. The authors argued that the diatomaceous ooze would be relatively free from contamination from old carbon and corrected the AIO ^{14}C dates by subtracting a standard 1,300 yr marine reservoir

(MRE) (e.g., Berkman and Forman, 1996). This approach was supported by relative palaeointensity (RPI) dating indicating that the inner shelf was ice free sometime before c.12,000-12,700 cal yr BP (Hillenbrand et al., 2010a).

The timing of deglaciation in the western ASE is broadly consistent with very sparse ^{14}C data from the eastern ASE. On the mid-shelf, west of Burke Island, calcareous foraminifera found in glacial-marine sediment overlying till yielded an age of 14,500 ± 3,900 ^{14}C yr BP (corrected age; Lowe and Anderson, 2002. We quote the calibrated age of 17, 450 cal yr BP given in Heroy and Anderson, (2008) but note that the calibrated age could lie between 12,750-22,000 cal yr BP if the full error is used in the calibration). An additional date, from the base of a glaciomarine sequence, which did not recover till, yielded a minimum age of 8,850 ^{14}C yr BP for deglaciation further inshore (corrected age; Lowe and Anderson, 2002), although the core site still lies 190 km from the modern ice front of PIG. Thus, the sparse ^{14}C data from the ASE suggest that the western mid to inner shelf deglaciated between c. 9,950-17,400 cal yr BP, while deglaciation of the inner part of Pine Island Bay is still poorly constrained.

3. Methodological approach

3.1. Sedimentary facies and dating the retreat of grounded ice

Cores recovered from palaeo ice-stream troughs on the Antarctic continental shelf typically yield a three-fold sediment stratigraphy with a largely homogenous diamicton (subglacial facies) at the base overlain by stratified to structureless, sandy to gravelly, terrigenous sediments (transitional or deglacial facies), which in turn are overlain by bioturbated to homogenous, diatom- or foraminifera-bearing glaciomarine muds (open marine facies) (Domack et al., 1999, 2005; Evans and Pudsey, 2002;

Dowdeswell et al., 2004a; Evans et al., 2005; Heroy and Anderson, 2005; 2007; Ó Cofaigh et al., 2005; Pudsey et al., 2006; Heroy et al., 2008; Hillenbrand et al., 2005, 2009, 2010b). Typically the subglacial diamicton was deposited by fast flowing ice streams as deformation till, the transitional sediments, which mark the phase of ice lift off at the core site, were deposited proximal to the grounding line (GL) and the microfossil-bearing glaciomarine muds in an open-marine (hemipelagic) setting directly following ice retreat. This three-fold stratigraphy represents the most reliable sediment sequence for establishing retreat of grounded ice as it records the transition from subglacial deposition through to open marine conditions (e.g., Heroy and Anderson, 2007). However, due to the scarcity of radiocarbon data in Antarctica it is sometimes necessary to report dates from other stratigraphies, such as those which only recovered the transitional and open-marine facies, iceberg turbates, winnowed coarse-grained deposits (so-called 'residual glaciomarine sediments'), gravity-flow deposits and iceberg-rafted diamictons.

Unfortunately, Antarctic shelf sediments generally lack calcareous foraminifera, which are conventionally used for radiocarbon dating and have well-defined reservoir corrections (e.g., Berkman and Forman, 1996). When carbonate (micro-)fossils are absent it is necessary to date the 'bulk' or acid insoluble organic (AIO) fraction. However, these 'bulk' AIO ages are subject to significant contamination from relict organic matter eroded from the Antarctic continent (Licht et al., 1996; Andrews et al., 1999; Ohkouchi and Eglinton, 2006) or re-working of older shelf sediments (Domack et al., 1999), which can lead to substantially older radiocarbon ages. Despite this problem, several studies have successfully utilized ages from the AIO fraction to establish deglacial chronologies for the Antarctic shelf (Licht et al., 1996; 1998; 1999; Domack et al., 1999; Pudsey and Evans, 2001; Licht and

Andrews, 2002; Heroy and Anderson, 2005; 2008; Mosola and Anderson, 2006; McKay et al., 2008; Hillenbrand et al., 2010a, b).

An additional complication often relates to which sedimentary unit should be dated. Heroy and Anderson (2007) have recently argued that the lowermost transitional facies should be dated rather than the lowermost open marine facies because a time-lag will exist between lift-off of grounded ice and onset of hemipelagic sedimentation. However, like previous authors (e.g., Pudsey and Evans, 2001; Pudsey et al., 2006), Heroy and Anderson (2007) observed that samples in the lowermost transitional facies were significantly older than samples taken from the interface between the transitional and open marine facies. This drastic downcore increase of ages results in a so-called '^{14}C dog-leg' (see Figure 2e in Heroy and Anderson, 2007) in age-depth profiles where the abrupt increase in ^{14}C age with depth is related to a higher degree of contamination from fossil organic carbon in the transitional unit (Heroy and Anderson, 2007). Hillenbrand et al. (2009, 2010b) found a similar pattern in the Bellingshausen Sea and suggested that the clay mineral assemblage of shelf cores can be used as a detector to help pinpoint the most suitable horizon to date in each core. The authors showed that the lower section of the transitional facies often contains a clay mineralogical assemblage more similar to the subglacial facies, implying most contamination, whilst the upper section of the transitional facies contains a clay mineral assemblage similar to the open-marine facies. On the basis of this relationship Hillenbrand et al. (2010b) argued that the most reliable deglaciation ages are obtained from the upper part of the transitional facies/lower part of the open marine facies because it reflects the decreasing influx of (potentially contaminated) sediments delivered to the grounding line and increasing influence of modern (open-marine) sedimentation.

3.2. Criteria for selecting samples for ^{14}C dating

In order to achieve the most reliable deglacial chronology for the western ASE we implemented a rigorous dating strategy whereby detailed sedimentological, physical properties and geochemical data were used to select the horizon in each core that would yield the most reliable AIO ^{14}C deglacial age (i.e., a date free from major contamination with old carbon while still representing the passing of the grounding line across the core site). In cores with a three-fold stratigraphy, samples for dating ice-sheet retreat were taken directly above the contact between the transitional and the open marine facies (Fig. 2a, Suppl. Fig. 1). This boundary was identified using distinct changes in grain-size (typically a down-core change from gravel/coarse sand to silt and clay to gravel/coarse sand), changes in magnetic susceptibility (either a downcore increase or decrease, probably depending on changes in magnetic provenance), a down-core increase in shear strength and changes in the clay mineral assemblage. In cores that recovered open-marine sediment directly overlying the subglacial facies, the samples for ^{14}C dating the ice-sheet retreat were taken from the lower part of the open-marine facies (Suppl. Fig. 1).

We consider our approach to provide the most reliable age for deglaciation, when using conventional AMS ^{14}C dates from the AIO fraction. Furthermore, whilst the transitional facies spans the time period between the first stage of deglaciation (i.e., lift-off of grounding ice) and the onset of seasonal open-marine sedimentation, we argue that unless there is clear evidence for the presence of a large ice shelf (see Kilfeather et al., in press) the calving margin will closely follow retreat of the GL. As such, the date we provide for deglaciation is a minimum age for GL retreat, but one that we consider to be robust and relatively free from contamination. Thus, in the context of this paper, we use the term deglaciation to refer to the onset of glaciomarine influence (here defined as the recognition of the first influence by glaciomarine processes after the passage of the GL over the core site). Additional samples for ^{14}C dating were taken either side of this 'optimum horizon' to investigate presence of significant age reversals/changes in sedimentation and to ensure that samples for dating the deglaciation were taken from above any pronounced ^{14}C dog-leg. We also routinely dated the AIO of surface sediments at each core site to correct downcore AIO ages, and also dated calcareous (micro-)fossils wherever this was possible.

4. Material and methods

4.1. Sample collection and laboratory analyses

Geophysical data and sediment cores were collected during cruise JR141 of the RRS *James Clark Ross* (*JCR*) and ANT-XXIII/4 of RV *Polarstern* (*PS*) in 2006. Swath bathymetry data were obtained on *JCR* using a Kongsberg EM120 system with 191 beams in the 11.25–12.75 kHz range and on *PS,* using an Atlas Hydrosweep DS-2 system with 59 beams at 15.5 kHz. Detailed swath bathymetry data are published in more detail elsewhere (Nitsche et al., 2007; Larter et al., 2007; 2009; Graham et al., 2009). Sediment cores were collected along transects within the three tributary troughs and the main trough (Fig. 1a & b) using a vibrocorer (VC) and gravity corer (GC), whilst surface sediments were collected using a box corer (BC) and giant box corer (GBC), respectively (Table 1). Surface samples, representing the sediment-water interface, were sampled directly from the box together with up to three sub-cores. Physical properties (magnetic susceptibility, wet bulk density (WBD), and P-wave velocity) were measured on whole cores using GEOTEK multisensor core loggers (MSCL) at the British Ocean Sediment Core Research Facility (BOSCORF, Southampton, UK) and at the Alfred Wegener Institute (AWI, Bremerhaven, Germany). Magnetic susceptibility was additionally measured on the split halves of the cores using a BARTINGTON MS2F point sensor at the British Antarctic Survey (BAS, Cambridge, UK) and at AWI. X-radiographs were obtained on whole core sections of the VCs and 1 cm-thick sediment slabs sampled from the GCs to investigate sedimentary structures. Shear strength was measured every 10-20 cm on the split cores using a hand held shear vane. Individual sediment sub-samples (1 cm-thick slices) were then taken every 5-20 cm and used to determine water content, grain size, total carbon (TC), organic carbon (C_{org}) and total nitrogen (N_{tot}). C_{org} and N_{tot} were determined using element analyzers LECO CS-125, CS-400 and CNS-2000 at AWI and Vario EL III Elemental analyser at the Institute for Geophysics and Geology (University of Leipzig, Germany) and used to calculate C_{org}/N_{tot} ratios. Analytical precision was 1% for the TC measurements and 3% for the C_{org} measurements. We also calculated calcium carbonate ($CaCO_3$) contents from the TC and C_{org} data. For grain size analyses sediment samples were disaggregated in deionised H_2O and then passed through a 2 mm and a 63µm sieve. The <63 µm fraction was then treated to 20% hydrogen peroxide solution and 10% Hydrochloric acid, to remove C_{org} and $CaCO_3$ and dispersed in 2 ml of Sodium Hexametaphosphate ($(NaPO_3)_6$). The grain-size distribution of the <63 µm fraction was determined using a MALVERN microplus 5100 mastersizer at BAS, a Laser Granulometer LS230 equipped with a fluid module and PIDS (Polarisation Intensity Differential Scatter) attachment at the Department of Geography (University of Durham, UK) and a Micrometrics SediGraph 5100 at the Department of Geology (University of Tromsø, Norway). The proportions of the sand, silt, and clay fractions (< 2 mm) were determined on a weight basis.

An aliquot of the ≤2 μm fraction was used to determine the relative contents of the clay minerals smectite, illite, chlorite and kaolinite in core and surface samples using an automated powder diffractometer system Rigaku MiniFlex with CoKα radiation (30 kV, 15 mA) at the Institute for Geophysics and Geology (University of Leipzig). The clay mineral identification and quantification followed the standard X-ray diffraction methods described by Ehrmann et al. (1992) and Petschick et al. (1996), and as utilised in Ehrmann et al. (in review). For supplementary data see http://doi.pangaea.de/XYZ.

4.2. ^{14}C Dating, correction and calibration

AMS ^{14}C dating was carried out at the NERC Radiocarbon Laboratory (Environment) in East Kilbride (UK). Where present, we dated calcareous material (c. 10 mg), mainly planktonic foraminifera tests of *Neogloboquadrina pachyderma* sinistral and benthic foraminifera tests picked from 1-2 cm thick sediment slices, because these ^{14}C dates provide the most reliable radiocarbon ages (e.g. Domack et al., 2005; Heroy & Anderson, 2007; Rosenheim et al., 2008). In total we dated 15 surface (AIO=13, foraminifera=2) and 63 (AIO=53, foraminifera=10) downcore samples. In line with previous studies (e.g., Andrews et al., 1999; Licht et al., 1998, 1999; Domack et al., 1999; Pudsey and Evans, 2001; Heroy and Anderson, 2005; 2008; Mosola and Anderson, 2006; Pudsey et al., 2006; Hillenbrand et al., 2010b) all downcore AIO ages were corrected by subtracting the uncorrected core-top age obtained from the BC surface sample. This assumes that the core top age represents modern deposition and is supported by ^{210}Pb data from core PS69/275-2, which indicates modern deposition (Hillenbrand et al., 2010a). In six cores (VC424, VC425, VC427, PS69/273, PS69/274, PS69/275), we dated relatively pure diatomaceous ooze samples. As noted above (section 2), we corrected all diatom ooze ages using the standard Antarctic MRE correction of 1,300 years (see Hillenbrand et al., 2010a, for further discussion).

Only two surface samples (BC431, BC435) and three vibrocores (VC419, VC436 and VC430) contained sufficient carbonate material for dating. For the surface samples it was possible to pick mono-specific *N. pachyderma* sin. tests, whilst the downcore samples comprised mixed planktonic and benthic species. These samples were corrected by subtracting a 1,300-year MRE (Berkman et al., 1998; Berkman and Forman, 1996; Harkness and Gordon, 1992; cf. Anderson et al., 2002).

Both the AIO core top and MRE corrections were applied prior to calibration (see Table 2). All dates were calibrated to calendar years before present (BP; relative to AD 1950) with the CALIB v5.1beta program using the Marine04 age model (Stuiver et al., 2005). We report all ages as either ^{14}C yr or calibrated years BP (cal yr BP) and note, where appropriate, if previously published ages are corrected, uncorrected or calibrated.

5. Results and interpretation

5.1. Facies analysis

Sediment facies were determined on the basis of visual core descriptions, x-radiographs, shear strength, physical properties (MS, WBD), grain-size, C_{org} and $CaCO_3$ contents, C_{org}/N_{tot} ratios and clay mineral assemblages (see Suppl. Table 1). These data were used to: (a) establish the depositional environment; and (b) select the optimum horizon in each core to date the deglaciation. We only display the smectite/chlorite ratios, as this ratio proved to be the most sensitive indicator of changes in sedimentary facies. Representative core logs and data are presented for each facies in Figure 2, with the corresponding data for all other cores given in Supplementary Figure 1. Our interpretations of sediment facies are consistent with previously published data from the Antarctic shelf (e.g. Licht et al., 1996, 1998, 1999; Domack et al., 1998, 1999; Anderson, 1999; Pudsey and Evans, 2001; Evans and Pudsey, 2002; Evans et al., 2005; Heroy and Anderson, 2005; Hillenbrand et al., 2005, 2009, 2010b; Ó Cofaigh et al., 2005; Smith et al., 2009).

5.2. Facies 1, 2 and 3

Cores VC408, VC415, VC418, VC424, VC425, VC427, PS69/273-2 and PS69/275-1 contained three distinct facies (Facies 1-3) interpreted as open marine, transitional (i.e. grounding-line proximal) and subglacial, respectively, whilst cores PS69/274-1 and PS69/267-1 contained only the transitional and the open marine facies (Facies 1-2) and cores VC417, VC428, PS69/280-1, PS69/265-3 and PS69/259-1 contained the open-marine facies directly overlying the subglacial facies (Facies 3 and 1) (Fig. 2 and Suppl. Fig. 1). These facies sequences represent the most reliable stratigraphic successions for dating glacial retreat (c.f., Heroy and Anderson, 2007).

Facies 3 typically comprises a massive, matrix supported diamicton with subangular to subrounded cobbles in a muddy matrix. Generally, the diamicton is grey to olive grey (predominantly 5Y 5/2, but also 5Y 5/1 gray to 5Y 4/1 dark gray) (Fig. 2). Shear strength ranges from 5–24 kPa and generally decreases towards the top of the diamicton. MS (200-1500 $x10^{-5}$ SI Units) and WBD (>1.6 g/ccm) are usually high, whilst water content is low (<35 wt.%). Grain-size composition is variable, but is generally characterised by 45-70% mud, 20-40% sand and 5-15% gravel, although some cores (e.g., PS69/280-1) contain up to 20% gravel. C_{org} content is generally low (c. 0.2 wt.%), whilst C_{org}/N_{tot} values are higher (>20) than in Facies 2 and 1. $CaCO_3$ content shows no consistent trend with values between 1 and 3 wt.%. In some cores, $CaCO_3$ content is highest in the diamicton (e.g., PS69/275-1).

We interpret Facies 3 as a deformation or 'soft till' deposited beneath fast flowing (streaming) ice. Facies 3 was mainly sampled in cores on the inner and mid-shelf, coinciding with elongated glacial lineations, indicative of ice-streaming on a mobile and deformable bed (Ó Cofaigh et al., 2007; King et al., 2009).

Facies 2 represents a transitional unit from Facies 3 to Facies 1 (Fig. 2, Suppl. Fig. 1). MS values, WBD and shear strength all decrease up-core, whilst water content increases. The 63µm-2 mm and >2 mm fractions also generally decrease up-core together with the C_{org}/N_{tot} ratios, while the C_{org} contents generally increase. In cores VC415 and PS69/273-2 the C_{org} values are lowest in the transitional facies. Generally, Facies 2 is similar in colour to Facies 3 (predominantly 5Y 5/2 to 5Y 4/1) whilst x-radiographs often show parallel to sub-parallel stratification and random to horizontal pebble orientation. Smear slides occasionally show a relative up-core increase in fragments of diatoms.

Facies 2 was probably deposited in a glaciomarine environment proximal to the grounding line of the ice stream, subsequent to its retreat from the core site (e.g., Domack et al., 1998, 1999; Licht et al., 1999; Evans and Pudsey, 2002; Hillenbrand et al., 2005, 2010b). The unit varies in thickness from c. 15 to 40 cm, but is absent in some cores.

Facies 1. The uppermost stratigraphic unit consists of an olive grey (5Y 4/2) to olive (5Y 4/3) massive, bioturbated diatomaceous to diatom-bearing mud, which ranges in thickness from 3 (VC425) to 226 cm (VC427). Planktonic foraminifera constitute the biogenic components in Facies 1 on the outer shelf (VC430, VC436) and were also observed at the core top of VC428 on the mid-shelf (Fig. 2, Suppl. Fig. 1). Shear strength and MS values are typically low (1-4 kPa and 10-80 x 10^{-5} SI Units respectively), whilst the <2 mm grain-size fraction is characterised by high clay and silt and low sand concentrations. Water and C_{org} content are high in Facies 1. Predominantly subangular to subrounded pebbles are occasionally present and interpreted as iceberg-rafted debris (IRD). Facies 1 is either structureless or shows burrows and mottles caused by bioturbation. The contact between the Facies 2 and Facies 1 ranges from sharp to gradational.

Facies 1 reflects deposition in a seasonally open marine setting, distal from the ice front. This interpretation is based on the presence of diatoms and/or planktonic foraminifera and bioturbation and is supported by the low concentration of coarse-grained material, high water content and low shear strength. In an earlier publication, we argued that the thick diatomaceous ooze that directly overlies the ice-proximal Facies 2 at some sites (PS69/273-2, PS69/274-1, PS69/275-1, VC424, VC425 and VC427) represented a period of enhanced productivity immediately after deglaciation, in a relatively warm, well-stratified ocean (Hillenbrand et al., 2010a). We also argued that ^{14}C ages from this unit would be relatively free from contamination with fossil carbon because of the apparent lack of terrigenous material and therefore most suitable for dating.

5.3. Other facies types included in our deglacial model

Due to the dearth of ^{14}C data from this area, we also incorporate some ages from other sedimentary facies sequences, such as iceberg turbates/iceberg-rafted diamictons (Facies 4) and proglacial gravity-flow deposits (Facies 5), into our deglacial chronology.

Facies 4: Cores VC436 VC430, VC436, PS69/283-5/6 recovered homogenous, grey (predominantly 5Y 4/1, but also 2.5Y 4/2 and 5Y 4/2) diamictons with uniformly high MS and WBD values, and low water content (<30 wt.% and commonly 18-20 wt.%). Shear strength values are generally high (up to 35 kPa), but can vary significantly downcore. C_{org} contents are generally low (<0.25 wt.%), whilst the $CaCO_3$ content varies between 1 and 3 wt.%. VC430 and VC436 occur on the outer shelf (<450 m water depth), whilst PS69/283-5/6 is located on a shallower trough flank on the middle shelf, in areas where multibeam bathymetry data show iceberg scours (see Fig. 11 in Graham et al., 2009). Based on their sedimentological characteristics and location within areas of iceberg scours, we interpret these deposits as a sequence of iceberg-rafted diamictons and iceberg turbates deposited after grounded ice had retreated. The high and variable shear strength most likely results from pervasive scouring and mixing of the seafloor sediments by icebergs.

In cores VC436 and VC430 calcareous foraminifera occur in low abundances throughout the diamictons and at several depths, enough planktonic and/or benthic foraminifers were present to obtain ^{14}C ages (Table 2). The presence of foraminifera in significant abundances, particularly of planktonic *N. pachyderma* sin. tests implies that the outer shelf was free of grounded ice at the time of their deposition, although we cannot rule out that advection beneath an ice shelf played a role (cf. Hemer et al., 2007).

In core VC436, all but one of the six downcore ^{14}C ages occur in stratigraphic order (Fig. 2c) with an age of 14,975 ± 46 ^{14}C yr BP (16,266 cal yr BP) at 540 cmbsf core depth. However, a significantly older age (20,115 ^{14}C yr BP, 22,351 cal yr BP) at 60 cmbsf, supported by replicate analysis of material from 61 cmbsf (18,080 ^{14}C yr BP, 19,945 cal yr BP) suggests some sediment re-working and re-distribution has taken place. We suggest that the age-reversal at 60-61 cmbsf depth results from the reworking of nearby sediments by an iceberg that ploughed older material over the site sometime after 9,941 ^{14}C yr BP (9,731 cal yr BP). Generally however, turbation by icebergs must have been relatively shallow to preserve discrete foraminiferal layers in stratigraphic order.

We also interpret similar deposits recovered at core sites PS69/283-5/6, which are also found in areas of iceberg scours (Fig. 11 in Graham et al., 2009), as iceberg-rafted diamictons/iceberg turbates. However, PS69/283-5/6 did not include calcareous micro-fossils so is not included in our deglacial model.

Facies 5 (VC419, VC422, VC411): Core VC419 recovered a sequence of homogenous, purely terrigenous silty-clay beds (predominantly 5Y 5/1 grey) characterised by low MS values and high water content intercalated with six discrete, 6-70 cm thick, terrigenous sand and/or gravel layers (predominantly 5Y 4/1 dark grey) with high MS values and low water content (Smith et al., 2009; Suppl. Fig. 1e). The two sandy gravel layers have sharp basal boundaries, are normally graded and capped by finely laminated sand and silt layers. The top 30 cm of the upper sandy gravel layer is strongly bioturbated. The upper three sand layers are also slightly bioturbated, have sharp basal boundaries and consist of well-sorted muddy sand. Shear strength is relatively low (c. 5 kPa) throughout the sequence, but is slightly higher at its base (c. 10 kPa). Arenaceous benthic and calcareous benthic and planktonic foraminifera occur within the basal sandy gravel layer between 384-380 cmbsf, which provided an uncorrected age of 11,237 ± 40 ^{14}C yr BP (11,432 cal yr BP).

Core site VC419 occurs in a deep, steep sided subglacial meltwater channel, which has probably been formed over several glacial cycles (Smith et al., 2009). In an earlier study, Smith et al. (2009), suggested that the sedimentological properties of the coarse-grained layers in core VC419, such as sharp basal boundaries with normal grading, are typical of gravitational down-slope transport (e.g., Lowe, 1982; Bartek and Anderson, 1991). Accordingly, we interpreted the layers as grain-flow deposits and coarse-grained turbidites, which were probably re-deposited from topographic highs, forming the flanks of the channel, since the LGM. Our interpretation is also supported by the presence of calcareous foraminifera in the sandy gravel layers of core VC419. *In situ* surface sediments from the deep inner shelf basins in the Amundsen Sea and the nearby Bellingshausen Sea are virtually carbonate-free (Hillenbrand et al., 2003) as a result of their location below the carbonate compensation depth (CCD), which is typically shallower than 500 m on the West Antarctic shelf (e.g., Li et al., 2000). The water depth of site VC419 (806 m) is well below the CCD, so the occurrence of calcareous foraminifera in the basal sandy gravel layer implies reworking and rapid burial of sediments from shallower water depths, probably by grain flows and/or turbidity currents deposited subsequent to deglaciation.

Terrigenous, massive and sometimes stratified muds, sands and gravels were also recovered at two other sites (VC422 and VC411; Fig. 2d and Suppl. Fig 1b). However, in contrast to VC419, these deposits did not contain calcareous (micro-)fossils and are therefore not included in our deglacial model.

5.5. ^{14}C Data

All uncorrected, corrected and calibrated radiocarbon ages are presented in Table 2. Uncorrected surface sample ages range from 1,693 to 2,768 ^{14}C yr BP (foraminifera) and 3,262 to 6,429 ^{14}C yr BP (AIO) and reflect the well-documented problems associated with sediment re-working/winnowing and introduction of old, fossil carbon, respectively (Fig. 3). Our AIO-derived surface ages are similar to those previously reported from the Ross Sea that yielded AIO ages in the range of 2,000–5,000 ^{14}C yr BP (Licht et al., 1996; Andrews et al., 1999; Domack et al., 1999; Licht and Andrews, 2002; Mosola and Anderson, 2006) and from the southern Bellingshausen Sea that yielded AIO ages from 3,800-6,400 ^{14}C yr BP (Hillenbrand et al., 2010b). Spatially, there appears to be no consistent pattern in the distribution of surface ages in the western ASE, although surface ages in the Dotson trough appear to be slightly older, perhaps reflecting a greater proportion of old carbon-bearing rocks beneath its catchment (Fig. 3; Ehrmann et al., in review).

Downcore (uncorrected ^{14}C) ages range from 4,919 to 20,115 ^{14}C yr BP for carbonate and 5,945 ^{14}C yr BP to 37,223 ^{14}C yr BP for the AIO fraction (Table 2). When corrected and calibrated, all downcore ages, with the exception of dates from cores VC424 and VC436 (discussed in more detail below), occur in stratigraphic order (within 1 σ error).

6. Interpretation of ^{14}C ages

6.1. Timing of deglaciation in the western ASE

Detailed mapping of subglacial bedforms in the western ASE indicate that streaming ice flowed along the three tributary troughs (Dotson, Getz A and B) converging into one large cross shelf trough around 73°30'S (Fig. 1) that extended to the shelf break (see Graham et al. (2009) for additional information). Highly elongate MSGL north of 73°30'S imply flow acceleration in the zone of ice convergence between the three troughs, which also coincides with the transition between acoustic basement and dipping sedimentary strata (Larter et al., 2009; Graham et al., 2009). Below we present minimum ages for the timing of grounded ice retreat along the main palaeo ice stream and the three feeder trough(s).

Figure 4a shows the calibrated ages plotted against distance from the modern-day grounding line (GL) for the western ASE (GL inferred from the MODIS dataset; Bohlander and Scambos, 2007). For cores recovered from the zone of ice-flow convergence between tributary troughs (e.g., VC424; Fig. 1) and those on the outer shelf (e.g., VC430, VC436) a mean distance relative to the GL of all relevant tributary troughs was calculated. Our most 'reliable' deglacial ^{14}C ages, represented by closed circles in Figure 4, were obtained from (1) the lowermost part of the seasonal open-marine sediments of Facies 1 (most sites), (2) the gravity flow deposit of Facies 5 (VC419), or (3) the iceberg-related deposits of Facies 4 (VC430, VC436). All these ages plot above any apparent ^{14}C dog-leg in the age-depth plots (Fig. 2 and Suppl. Fig. 1.). Ages that do not meet these criteria are excluded from our deglacial chronology, irrespective of how they fit with nearby ages. Furthermore, for all AIO deglacial ages, the corresponding samples were taken from sediments with relatively low C_{org}/N_{tot} ratios (<20), i.e. comparable to the C_{org}/N_{tot} ratios in the surface sediments. This approach ensures that the samples used for dating the deglaciation i) did not contain significantly more fossil organic carbon than those used for the downcore correction of the ^{14}C AIO dates and ii) were dominated by marine organic matter, which typically has C_{org}/N_{tot} ratios between 4 and 10, but may reach higher ratios (≤30) in Antarctic shelf environments (see references in Hillenbrand et al., 2010b).

Open circles of the same colour in Figure 4a relate to all other ages obtained from each core. These ages were mainly used to assess downcore consistency in ^{14}C ages (age reversals etc.) and assess the presence of apparent ^{14}C dog legs (see Fig. 2 and Suppl. Fig. 1). Figure 4b only shows our most reliable deglaciation ages, illustrating a consistent pattern (within error) of ice-sheet retreat from the shelf. Where more than one age from a core meets our criteria, only the oldest age is shown as a filled circle in Fig. 4b.

At sites PS69/274-1, PS69/275-1 and VC424, we also used the RPI records of the cores to identify the ^{14}C date providing the most reliable deglaciation age (see Hillenbrand et al., 2010a). On this basis, we reject ages from VC424 (276.5 cmbsf), VC425 (221 cm) and PS69/275-1 (228.5 cmbsf) as being too old (see Hillenbrand et al. 2010a for further discussion). We also note that the x-radiograph from core VC425 indicates that the upper part of the diatomaceous ooze layer sampled for dating (221 cmbsf) shows evidence of mixing with terrigenous material (visible as sand/terrigenous grains in the x-radiograph), whereas all other samples appear pure. This could explain why the age from VC425, as well as the basal ooze samples from VC424 and PS69/275-1 discussed above, are slightly older when compared to all other diatom ooze-derived ages. We therefore reject the ooze age from VC425 from our preferred deglacial model (Fig. 5).

Figure 4 shows that the deglaciation of the outer shelf is constrained by ages from core VC436, with the oldest age from VC436 occurring out of stratigraphic order (60 cmbsf; Fig. 2c). Whilst this age clearly indicates some degree of sediment reworking, probably by iceberg ploughing, the presence of both planktonic and benthic foraminifera at this depth implies that their deposition after the grounding-line had retreated. Thus, in the absence of additional data, we use this age (22,350 cal yr BP) as a minimum age for deglaciation of the outer shelf. Two foraminiferal ages from core site VC430 indicate ice-sheet retreat before c.11,000 cal yr BP (Table 2, Fig. 3).

Grounded ice had retreated along the main cross shelf trough (Fig. 1) to the mid-shelf south of 73°S by 13,837 cal yr BP (site VC428). From this location, the inner shelf appears to have deglaciated rapidly to positions close to the modern ice shelf fronts by 11,432 cal yr BP (VC419) to 10,072 cal yr BP (VC415) in the Dotson and Getz-A troughs respectively and perhaps as early as 12,618 cal yr BP (PS69/274-1) in the Getz B trough. In detail, we see that the timing and style of deglaciation is consistent between all three troughs (Fig. 5a-d), but subtle differences do exist. Except for one foraminiferal age from core VC419, all ^{14}C ages from the middle to inner shelf are derived from the AIO.

For each profile we present our favoured deglacial model (solid line), but retain all 'reliable' ages that meet our criteria to create a deglacial 'envelope' for the western ASE mid-inner shelf (Fig. 5d). This provides an upper and lower estimate for the minimum age for ice retreat (Table 3).

6.1.1. Dotson trough

Along the Dotson tributary trough, ice had retreated to within 12 km of the present ice shelf by 11,432 cal yr BP (Fig. 5a), with cores VC428, PS69/267-1, PS69/280-1, VC419 and VC417 showing a consistent pattern of retreat. In contrast, the age from core site VC408 indicates the onset of open marine influence occurred approximately 600 years later than at the more southerly core site of PS69/280-1 (Fig. 5a). Given our potential dating uncertainty (both laboratory error and ^{14}C correction and calibration), we retain this age as a minimum for deglaciation on this part of the shelf (Table 3), but omit it from our favoured deglacial profile. Core VC418, located between core sites PS69/280-1 and VC419 (Fig. 4a), also records a much later date for the onset of open marine influence, but we omit this date from our deglacial model, because no surface AIO age is available for this station. To correct the downcore age from VC418 we used the surface age from nearby core VC408, and this appears to have resulted in an anomalously young age.

Multibeam data from the Dotson tributary trough show a series of grounding zone wedges (GZW) (see Graham et al., 2009) formed on the inner shelf between core sites PS69/267-1 and PS69PS69/280-1. Glacial lineations terminating at the crest of the GZWs indicate that they formed during a phase of ice margin retreat (Graham et al., 2009), when the grounding line stabilised, probably on local pinning points. Although we have insufficient data to determine the precise timing and duration of deglacial still-stands, cores to the north and south place a constraint c.1,650 years on the maximum duration of GZW formation, which is consistent with the time span estimated for the deposition of a GZW on the western Antarctic Peninsula shelf (Larter and Vanneste, 1995). However, based on a simple sediment flux calculation, Graham et al. (2010) argued that the GZW in the eastern ASE could have formed within 120 years, so the stillstands during deglaciation could be relatively short-lived, relating to effective sediment delivery during a punctuated but otherwise rapid deglaciation.

6.1.2. Getz A Trough

The deglaciation of Getz A trough is constrained by ^{14}C ages from five cores (Fig. 5b). Three of these cores (VC424, VC425 and VC427) contained an almost pure diatomaceous ooze unit directly above the ice proximal facies (Facies 2). In an earlier paper, we argued that the relatively low content of terrigenous detritus in this diatomaceous ooze (also recovered from the Getz B trough) offered the possibility to obtain downcore ages that were largely unaffected by contamination from terrigenous fossil carbon (Hillenbrand et al., 2010a). Indeed, the calibrated ages from cores VC424 and VC427, using a standard MRE correction (1,300 years) for the diatomaceous ooze samples and a surface age correction for all other samples, show a consistent downcore trend (within error; e.g., Fig. 2b and Supplementary Figure 1).

Figure 5b shows that deglaciation of the inner shelf, to within 10 km of the modern ice shelf front, was complete by 10,072 cal yr BP (core site VC415; Fig. 5b). This is c. 1,000-2,000 years later than similar positions in the Dotson and Getz B troughs. It is possible that locally grounded ice (perhaps from Wright Island) or an ice shelf persisted on this part of the inner shelf after grounded ice had retreated from the main tributary trough. We emphasise that we use this date (10,072 cal yr BP) as our minimum age of deglaciation of this part of the shelf.

6.1.3. Getz B Trough

The pattern and timing of deglaciation of the Getz B tributary trough is broadly consistent with that of the Getz A tributary trough (Fig. 5c). Minimum ages for deglaciation are provided by diatomaceous ooze ages from four cores, which also includes core VC424. Reconstructed palaeo flow lines (based on subglacial bedforms) indicate that ice from the Getz A and Getz B troughs converged to the north east of Wright Island (Fig. 1b and Graham et al., 2009), so it is appropriate to use VC424 in both Getz A and B tributary trough deglacial profiles. Although there is some scatter in the ages from the inner shelf basin, our favoured deglacial model indicates that ice retreated almost instantaneously from the middle to inner shelf (i.e. between VC424 and PS69/274-1). Ice had retreated to within 10 km of the modern ice shelf front by 12,618 cal yr BP (PS69/274-1), which is 1,000-2,000 years earlier than the deglaciation of the inner shelf in both the Getz A and Dotson troughs.

In summary, deglaciation of the western ASE was underway as early as 22,351 cal yr BP, and certainly before 16,267 cal yr BP reaching the mid-shelf by 13,837 cal yr BP and the inner shelf to within c.10-12 km of the present ice shelf front between 12,618 and 10,072 cal yr BP (Fig. 5d). We note that the spread of ages for deglaciation of the mid to inner shelf is largely consistent, which we have used to provide an upper and lower estimate for the minimum age for ice retreat (Fig. 5d and Table. 3). However, in the remainder of the discussion, we only refer to age profiles shown in Figures 5a-c.

7. Discussion

7.1. Deglaciation of the WAIS along the Pacific margin

Limited data from the eastern ASE (i.e., Pine Island Glacier Trough; Fig. 1, e.g. Graham et al., 2010) suggest that the deglaciation of the middle shelf began sometime around c. 17,400 cal yr BP (calibrated age given in Heroy and Anderson, 2007) with a minimum age for deglaciation of the middle to inner shelf around 9,948 cal yr BP (10,150 ± 370 ^{14}C yr BP uncorrected age; Lowe and Anderson, 2002). Further to the west in the Getz D trough (Wrigley Gulf) open-marine condition were established on the middle to inner shelf between 14,750 to 15,215 cal yr BP (Anderson et al., 2002) (Fig. 6).

In the western Antarctic Peninsula (AP) region, Heroy and Anderson (2007) showed a north-south trend in ice-sheet retreat on the outer shelf, with earlier deglaciation of the Antarctic Peninsula Ice Sheet (APIS) occurring at 17,340 cal yr BP in the Bransfield Basin at its northwestern tip, later deglaciation of outer Anvers Trough (located further south) by c.15,000-16,000 cal yr BP and deglaciation of outer Marguerite Trough further to the south by c.14,000 cal yr BP (Fig. 1, inset). The inner shelf of Marguerite Bay was ice free by c. 9,100 cal yr BP (Heroy and Anderson, 2007), with seemingly very rapid deglaciation of the outer to middle shelf sectors of Marguerite Trough (Kilfeather et al., in press). Recently published data from the Bellingshausen Sea suggest that the WAIS and APIS there might have retreated much earlier than from other parts of the West Antarctic shelf, with deglaciation of the outer shelf occurring as early as 30,000 cal yr BP reaching the mid-shelf by 23,600 cal yr

BP (Hillenbrand et al., 2010b). Deglaciation of the inner shelf areas occurred at 14,300 cal yr BP in Eltanin Bay and c. 7,200 cal yr BP in the Ronne Entrance (Hillenbrand et al., 2010b).

In the western and central Ross Sea, AIO ages on diatomaceous muds constrain the deglaciation of the outer shelf, south of Coulman Island, to c. 20,000-14,000 ^{14}C yr BP (corrected age; Bindschadler, 1998; Conway et al., 1999; Domack et al., 1999; Anderson et al., 2002; Licht and Andrews, 2002; Licht, 2004; Mosola and Anderson, 2006). After c. 16,390 cal yr BP (13,770 ^{14}C yr BP, corrected age; Licht and Anderson, 2002) grounded ice retreated southward across the shelf, reaching outer Drygalski Trough by c. 13,000 cal yr BP (11,060 ^{14}C years BP, corrected age; Domack et al., 1999), Ross Island by c. 11,700 cal yr BP (10,096^{14}C yr BP, corrected age; McKay et al., 2008), with open marine conditions being established north of Ross Island at c. 10,000 cal yr BP (8,861 ^{14}C years BP, corrected age; McKay et al. 2008). According to McKay et al. (2008) the ice shelf has been pinned to Ross Island since then, while the grounding line has continued to retreat towards the Siple Coast.

Our chronological data from the western ASE is broadly consistent with the previously published data from the eastern ASE and Wrigley Gulf (Anderson et al., 2002; Lowe and Anderson, 2002), but provides much more detailed constraints on the deglaciation of this sector of the WAIS, particularly on the mid- to inner shelf (Fig. 6). Specifically, we point to the close agreement between our mainly AIO-based deglacial ages and previously published carbonate deglacial ages for the inner shelf sector of the Getz-D system, which cluster around 14,000 cal yr BP (Anderson et al., 2002) (Fig. 6). The timing of deglaciation of the outer shelf in the western ASE at 22,351 cal yr BP, is considerably older than initial retreat of the APIS (17,500 cal yr BP) but is consistent with the onset of WAIS retreat from the outer shelves of the

Ross Sea (25,166 cal yr BP; Mosola and Anderson, 2006) and the Bellingshausen Sea (30,000 cal yr BP; Hillenbrand et al., 2010b). If correct, the deglacial ages from the western ASE/Bellingshausen Sea sector of the WAIS indicate deglaciation was underway earlier than previously thought (cf. Anderson et al., 2002). Generally, however, the deglaciation of the western ASE precedes the deglaciation of the western Ross Sea, which could reflect the proximity of the western Ross Sea to the Transantarctic Mountains. It has been previously suggested that the ice on the western Ross Sea shelf at the LGM was partly fed by ice flowing from the East Antarctic Ice Sheet (e.g. Licht et al., 2005), which is thought to have had a different retreat history from the WAIS (Anderson et al., 2002; Mosola and Anderson, 2006).

7.2. Timing of deglaciation in the western ASE and relation to global meltwater pulses (mwp)

An Antarctic source for global meltwater pulse (mwp) 1a and 1b has been suggested on the basis of both viscoelastic Earth models (e.g., Bassett et al., 2005; 2007) and limited geological data from the margins of the WAIS. Heroy and Anderson (2007) argued that the timing of deglacial steps of the APIS are roughly concomitant with mwp-1a (14,650-13,700 cal yr BP or 12,500- 11,800 ^{14}C yr BP) and possibly 1b (10,350-11,200 cal y BP or 9,200-9,800 ^{14}C BP; Fairbanks et al., 1989), but that the earliest APIS retreat occurred later (c.1000 years) than the 19 ka mwp (22,000-19,000 cal yr BP; Yokohama et al., 2000; Fig. 6). In addition, Hillenbrand et al. (2010b) suggested that the WAIS and APIS retreat from the southern Bellingshausen Sea shelf may have contributed to the 19 ka mwp, mwp-1a and mwp-1b, but was unlikely to have triggered them. In the Ross Sea, McKay et al. (2008)

argued that retreat of the grounding line from the outer Drygalski Trough to Ross Island is likely to have contributed to mwp-1b (Fig. 6), whilst a Ross Sea contribution to mwp-1a has been ruled out by Domack et al. (1999) and Licht (2004) with major retreat occurring at c. 11,000 ^{14}C BP.

The timing of deglacial steps in the western ASE is also coincident with meltwater pulses mwp-1a and mwp-1b (Fig. 6). Specifically, our data indicate a step in deglaciation from the mid- to inner-shelf that is roughly in phase with mwp-1a (Fig. 6), with the majority of rapid retreat shortly after c.14,000 cal yr BP (Fig 6). A minor step in the deglaciation of the inner shelf also occurs shortly before mwp-1b, but generally the timing of mwp-1b appears to coincide with an overall slowdown and stabilisation of ice retreat on the inner shelf in the western ASE. We also tentatively note that the initial rise in sea level associated with the 19 ka mwp, recorded at 22,000 cal yr BP (Yokohama et al., 2000) immediately follows the onset of deglaciation of the outer shelf in the western ASE(22,351 cal yr BP).

Despite an apparent correlation between the timing of deglaciation of the western ASE and global mwps, it remains difficult to fully assess such a relationship owing to the potential errors associated with current dating methods. Furthermore, the overall contribution of ice in the western ASE, whilst not insignificant, is a relatively small component of the whole sea-level budget. Bassett et al. (2007) estimated that ice from the entire ASE has contributed just 0.5 m to eustatic sea level since the LGM, with only 0.15 m contributing to mwp-1a, thus making it a relatively minor component of the 15 m of sea level rise associated with the global mwp-1a event.

Interestingly, the timing of mwp-1a coincides with ice-sheet retreat over the deep inner shelf basins of the Dotson and Getz tributary troughs (Fig. 7). Thus a possible mechanism for the rapid phase of ice retreat that we see in these areas might be the combined effect of a sudden sea-level rise associated with mwp-1a, together with instability at the grounding line as the ice sheet retreated across the reverse basal gradients on the inner shelf.

7.3. Long-term ice trajectories and rates of grounding line retreat – the role of deep inner shelf basins, pinning points and rising sea-level in rapid deglaciation

The trajectory of ice sheet retreat from the outer to the middle shelf of the ASE indicates an average grounding-line retreat of 18 m/yr (Fig. 7). This value contrasts markedly with ice-sheet retreat across the mid- to inner-shelf, which appears to have reached 140 to 400 m/yr along the Dotson trough. Retreat rates were not calculated for inner Getz A and B troughs because the dated unit (diatomaceous ooze) from these cores is likely to have been deposited synchronously after deglaciation (Hillenbrand et al., 2010a) (Fig. 7 and 8). Our calculated retreat rates for the mid- to inner shelf of the Dotson trough are comparable to both contemporary (450 m/yr between 1963-1992 for Ice Stream B; Bindschadler and Vornberger, 1998) and palaeo estimates (average retreat of 120 m/yr over the last 7,500 years; Conway et al., 1999) for ice sheet retreat in the Ross Sea but are higher than post glacial retreat rates in the Bellingshausen Sea (6-44 m/yr; Hillenbrand et al., 2010b). However, they are considerably lower than the recent, rapid GL retreat of Pine Island Glacier (PIG) (i.e., 1200 ± 300 m/year between 1992 and 1996; Rignot, 1998).

One explanation for the acceleration in GL retreat towards the inner shelf, seen in all three troughs could be the along trough bathymetric profiles in the western ASE, which show a pronounced deepening on the mid-shelf at around 73°S (i.e., c. 200 km from modern GL; Fig. 8). Thus, the acceleration of retreat could be related to the crossing of one or more geomorphic and/or glaciological thresholds. We suggest that as the GL retreated into the deeper water on the inner shelf, the calving flux increased leading to higher ice velocities and rapid ice sheet thinning and retreat (e.g., Long and Roberts, 2003; Benn et al., 2007; Schoof, 2007; Vaughan and Arthern, 2007; Briner et al., 2009). Also significant is the timing of ice retreat across the deep inner shelf, which coincides with the c.15 m of sea-level rise associated with mwp-1a (Fig. 8). Thus, it is possible the sudden rise in sea-level at c.14,000 cal yr BP contributed to a phase of rapid retreat, weakening further the drag between the ice sheet and its bed.

The reverse gradient and rougher topography of the inner shelf may have also exposed the base of the ice sheet to warm CDW, promoting greater melting at the base of the ice sheet/ice shelf cavity. CDW is currently delivered to the fringing ice shelves of the ASE along the deep palaeo ice-stream troughs (e.g., Walker et al., 2007) (Fig. 1), and has been implicated in the thinning of the floating portion of PIG, which in turn has been linked to rapid thinning, grounding line retreat and acceleration of PIG itself. Jenkins et al. (2010) argued that the recent retreat of PIG, whilst related to basal melting by CDW, is significantly controlled by the shape of the glacier bed, and specifically the passing of important pinning points. The authors demonstrated that PIG was grounded on a transverse ridge until the early 1970's and retreat from the ridge has exposed more than 30 km of previously grounded glacier base to melting by CDW. Jenkins et al. (2010) concluded that thinning of the ice shelf through basal melting is sustained by a positive feedback, whereby the drag between the ridge and ice shelf has been reduced, resulting in enhanced spreading and thinning of the ice shelf, and thus allowing more CDW over the ridge and into the ice shelf cavity. To maintain balance, the reduced drag is offset by higher tension at the GL, which leads to faster discharge of ice (Schoof, 2007) and dynamic thinning of the glacier. The sudden loss of drag, or pinning might help to explain the very rapid retreat rates observed for PIG.

We suggest a similar scenario for the deglaciation of the western ASE inner shelf, with sudden and rapid steps in GL retreat associated with the loss of pinning on a reverse gradient slope. In the eastern Amundsen Sea too, stepped phases of rapid grounding line retreat have been postulated on the basis of geomorphic evidence (Graham et al., 2010). In addition, the contact between the ice sheet and submarine topographic high points or ridges would have been weakened further by enhanced basal melting if CDW gained access to the sub-ice cavity.

The pace and ultimate extent of such 'unstable retreat' (Schoof, 2007) is ultimately dependent on the presence of local pinning points. For PIG, the grounding line is anticipated to retreat a further 200 km inland until it encounters the next cross trough ridge (see Fig. 2c in Jenkins et al., 2010). Although we cannot fully constrain ice retreat in the western ASE beyond the present ice shelf margin (the GL occurs approximately 65-90 km inland from the ice shelf front), our dataset suggests that the ice margin stabilised on the inner shelf during the early Holocene (e.g., between core site VC427 and VC415, Getz A trough; Fig. 8). If we assume monotonic retreat of the ice-sheet from the inner shelf to the current GL, this would equate to a retreat rate of c.7 m/yr, implying a significant slowdown in GL retreat sometime during the early Holocene. Presently the Dotson and Getz ice shelves are stabilised by lateral drag against the flanking coastal peninsulas and islands (Fig. 1), and it is possible that their formation, during the early Holocene, played an important role in stabilising the calving front. Although poorly mapped, bathymetric data (Le Brocq et al., 2010) indicate that the modern GL in the Dotson-Getz sector coincides with several topographic pinning points c. 350 m below sea-level, which are also likely to have helped stabilise the GL following the rapid retreat along the inner shelf troughs.

For ice buttressed by the Dotson Ice Shelf (e.g., Kohler Glacier), we speculate that additional phases of rapid retreat are possible as the reverse gradient of the Dotson A tributary trough, although dissected by several topographic highs (pinning points), appears to extend well into the interior of the WAIS. Thus, similar to what has currently been observed for PIG (e.g., Jenkins et al., 2010), continued basal melting of the Dotson Ice Shelf (e.g., Shepherd et al., 2010) could lead to rapid phases of GL retreat as new sub-ice cavities are exposed to warm CDW and greater basal melting. In contrast, the Getz B Ice shelf occupies an east-west trending trough, with the GL pinned to a well-defined topographic high at or close to modern sea level. As a result, it would take much more thinning of the ice sheet for the GL to retreat further inland.

7.4 Questions and future work

We have presented an extensive new chronological dataset for the western ASE, which fills an urgent requirement to provide a deglacial framework for retreat of the WAIS in this sector since the LGM. However, despite good core coverage on the middle to inner shelf, our deglacial chronology for the middle to outer shelf remains poorly constrained. Future expeditions to this area should aim to target the outer shelf, particularly in areas free from iceberg turbation/ploughmarks. Whilst we are confident in our chronological approach and dataset, the framework we have presented should be tested and refined by additional dating methods such as ramped pyrolysis (Rosenheim et al., 2008), compound specific dating (Ohkouchi and Eglinton, 2008) and additional RPI dating (e.g., Hillenbrand et al., 2010a). In addition, all cores should be closely inspected for carbonate remains, since dating carbonate offers the most accurate method for determining the retreat history of the LGM ice sheet. Finally, it is critical that we establish the onset of CDW upwelling onto the Amundsen Sea shelf, i.e. whether this occurred immediately after the deglaciation of the outer shelf or sometime during the Holocene. An answer to this question is significant, because it will help to constrain the role of basal melting in phases of rapid deglaciation and also clarify how long glaciers and ice shelves in this area have been subject to rapid basal melting and thinning.

8. Conclusion

- Detailed analysis of sediment cores from the western ASE, pre-selection of samples for ^{14}C dating, and comparison of the resulting dates with one obtained from carbonate samples, diatom oozes and RPI dating demonstrates that reliable ages for deglaciation of LGM ice sheet can be established using the AIO fraction. Our approach results in a minimum age for GL retreat, but one that we feel is robust and free from significant contamination. Upper and lower estimates of the minimum age for deglaciation are given in Table 3.
- Our extensive new ^{14}C dataset indicates that deglaciation of the outer shelf began sometime prior to 22,351 cal yr BP, reaching the mid-shelf by 13,837 cal yr BP and the inner shelf to within c.10-12 km of the present ice shelf front between 12,618 and 10,072 cal yr BP.
- The timing of deglaciation of the mid- to inner shelf is consistent with previously published carbonate ages from the Wrigley Gulf (Getz D area) as

well as the timing of ice stream retreat in Marguerite Trough. The ice-sheet retreat from the outer shelf in the western ASE appears to precede deglaciation of the western Ross Sea, which might suggest that ice retreat in the western Ross Sea was more closely coupled to retreat of the EAIS than the WAIS.

- The acceleration in grounding-line retreat from the middle to inner shelf coincides with a landward-increasing reverse gradient along the tributary troughs. Such acceleration of ice retreat could relate to detachment from pinning points on a reverse gradient slope (e.g., Schoof, 2007). A sudden rise in sea level (mwp-1a) at this time might also have contributed to the acceleration of GL retreat by further reducing the drag between the ice sheet and its bed.

9. Acknowledgements

This study is part of the British Antarctic Survey Polar Science for Planet Earth Programme (GRADES-QWAD and Palaeo-Ice Sheets work package), funded by The Natural Environment Research Council. Additional funding from the Alfred Wegener Institute MARCOPOLI Programme, the UK Natural Environment Research Council (NERC) New Investigator Grant NE/ F000359/1 and the Deutsche Forschungsgemeinschaft (grant to Werner Ehrmann) is also acknowledged. We wish to thank the expert technical help of NDT services (notably Ian Tomlinson and Zammo) for providing core x-rays and Jeremy Sothcott (BOSCORF) for help with core logging. In addition, we thank the captains, officers, crew, support staff and scientists who participated in cruises JR141 and ANT-XXIII/4. Finally the comments of Phil O'Brien and an anonymous reviewer are greatly appreciated and have helped improve the clarity of our paper.

10. References

Anderson, J.B., 1999. Antarctic Marine Geology. Cambridge University Press, Cambridge, p. 289.

Anderson, J.B., Shipp, S.S., Lowe, A.L., Wellner, J.S., Mosola, A.B., 2002. The Antarctic Ice Sheet during the Last Glacial Maximum and its subsequent retreat history: a review. Quaternary Science Reviews 21, 49–70.

Bartek, L.R., Anderson, J.B., 1991. Facies distribution resulting from sedimentation under polar interglacial climatic conditions within a high-latitude marginal basin, McMurdo Sound, Antarctica. Geological Society of America Bulletin 261, 27–49.

Andrews, J.T., Domack, E.W., Cunningham, W.L., Leventer, A., Licht, K.J., Jull, A.J.T., DeMaster, D.J., Jennings, A.E., 1999. Problems and possible solutions concerning radiocarbon dating of surface marine sediments, Ross Sea, Antarctica. Quaternary Research 52, 206–216.

Bassett, S.E., Milne, G.A., Mitrovica, J.X., Clark, P.U., 2005. Ice sheet and solid earth influences on far-field sea-level histories. Science 309, 925–928.

Bassett, S.E., Milne, G. A., Bentley, M.J., Huybrechts, P., 2007. Modelling Antarctic sea-level data to explore the possibility of a dominant Antarctic contribution to Meltwater Pulse IA. Quaternary Science Reviews 26, 2113–2127.

Benn, D. I., Warren, C. R., Mottram, R. H., 2007. Calving processes and the dynamics of calving glaciers. Earth Science Reviews 82, 143-179.

Bentley, M.J., 2009. The Antarctic palaeo record and its role in improving predictions of future Antarctic Ice Sheet change. Journal of Quaternary Science 25, 5-18.

Berkman, P.A., Forman, S.L., 1996. Pre-bomb radiocarbon and the reservoir correction for calcareous marine species in the Southern Ocean. Geophysical Research Letters 23, 363-366.

Berkman, P. A., Andrews, J. T., Björck, S., Colhoun, E. A., Emslie, S. D., Goodwin, I. D., Hall, B. L., Hart, C. P., Hirakawa, K., Igarashi, A., Ingólfsson, O., López-Martínez, J., Lyons, W. B., Mabin, M. C. G., Quilty, P. G., Taviani, M., and Yoshida, Y., 1998. Circum-Antarctic coastal environmental shifts during the Late Quaternary reflected by emerged marine deposits. Antarctic Science 10, 345-362.

Bindschadler, R., Vornberger, P., 1998. Changes in the West Antarctic Ice Sheet since 1963 from declassified satellite photography. Science 279, 689–692.

Biscaye, P.E., 1964. Distinction between kaolinite and chlorite in recent sediments by X-ray diffraction. American Mineralogist 49, 1281-1289.

Biscaye, P.E., 1965. Mineralogy and sedimentation of recent deep-sea clays in the Atlantic Ocean and adjacent seas and oceans. Geological Society of America Bulletin 76, 803-832.

Bockheim, J.G., Wilson, S.C., Denton, G.H., Andersen, B.G., Stuiver, M., 1989. Late Quaternary ice-surface fluctuations of Hatherton Glacier, Transantarctic Mountains. Quaternary Research 31, 229–254.

Bohlander, J., Scambos, T., 2007. Antarctic coastlines and grounding line derived from MODIS Mosaic of Antarctica (MOA). Boulder, Colorado USA: National Snow and Ice Data Centre. Digital media.

Brindley, G.W., Brown, G. (Eds.), 1980. Crystal Structures of Clay Minerals and their X-ray Identification. Mineralogical Society of London Monogrographs 5, London, 495 pp.

Briner, J.P., Bini, A.C., and Anderson, R.S., 2009. Rapid early Holocene retreat of a Laurentide outlet glacier through an Arctic fjord. Nature Geoscience 2, 496-499.

Clark, P.U., Mitrovica, J.X., Milne, G.A., Tamisiea, M.E., 2002. Sea-level fingerprinting as a direct test for the source of global Meltwater Pulse IA. Science 295, 2438–2441.

Conway, H., Hall, B.L., Denton, G.H., Gades, A.M., Waddington, E.D., 1999. Past and future grounding-line retreat of the West Antarctic Ice Sheet. Science 286, 280–283.

Denton, G.H., Hughes, T.J., 2000. Reconstruction of the Ross ice drainage system, Antarctica at the last glacial maximum. Geografiska Annaler 82A, 143–166.

Domack, E., O'Brien, P., Harris, P., Taylor, F., Quilty, P.G., De Santis, L., Raker, B., 1998. Late quaternary sediment facies in Prydz Bay, East Antarctica, and their relationship to glacial advance onto the continental shelf. Antarctic Science 10, 236-246

Domack, E.W., Jacobsen, E.A., Shipp, S.S., Anderson, J.B., 1999. Late Pleistocene – Holocene retreat of the West Antarctic ice sheet system in the Ross Sea: a new perspective: Part 2, Sedimentologic and stratigraphic signature. Geological Society of America Bulletin 111, 1517– 1536.

Domack, E., Duran, D., Leventer, A., Ishman, S., Doane, S.S., McCallum, S., Amblas, D., Ring, Gilbert, R., Prentice, M., 2005. Stability of the Larsen B ice shelf on the Antarctic Peninsula during the Holocene epoch. Nature 436, 681-685.

Dowdeswell, J.A**.**, Ó Cofaigh, C. and Pudsey, C.J., 2004a. Thickness and extent of the subglacial till layer beneath an Antarctic paleo-ice stream. Geology 32, 13-16.

Dowdeswell, J.A., Ó Cofaigh, C., Pudsey, C.J., 2004b. Continental slope morphology and sedimentary processes at the mouth of an Antarctic palaeo-ice stream. Marine Geology 204, 203– 214.

Ehrmann, W.U., Melles, M., Kuhn, G., Grobe, H., 1992. Significance of clay mineral assemblages in the Antarctic Ocean. Marine Geology 107, 249-273.

Ehrmann, W., Hillenbrand, C.-D., Smith, J.A., Graham, A.G.C., Kuhn, G., Larter, R.D., Provenance changes between recent and glacial-time sediments in the Amundsen Sea Embayment, West Antarctica: clay mineral assemblage evidence [in review Antarctic Science].

Evans, J., Pudsey, C.J., 2002. Sedimentation associated with Antarctic Peninsula ice shelves: implications for palaeoenvironmental reconstructions of glaciomarine sediments. Journal of the Geological Society 159, 233-237.

Evans, J., Pudsey, C.J., Ó Cofaigh, C., Morris, P., Domack, E., 2005. Late Quaternary glacial history, flow dynamics and sedimentation along the eastern margin of the Antarctic Peninsula Ice Sheet. Quaternary Science Reviews 24 (5-6), 741-774.

Fairbanks, R.G., 1989. A 17,000-year glacio-eustatic sea level record: influence of glacial melting rates on the Younger Dryas event and deep-ocean circulation. Nature 342, 637–642.

Fairbanks, R.G., Mortlock, R.A., Chiu, T-C., Cao, L., Kaplan, A., Guilderson, T.P., Fairbanks , T.W., Bloom, A.L., 2005. Marine Radiocarbon Calibration Curve Spanning 0 to 50,000 Years B.P. 2005. Based on Paired ^{230}Th/^{234}U/^{238}U and ^{14}C Dates on Pristine Corals. Quaternary Science Reviews 24, 1781-1796

Gordon, J. E., Harkness, D. D., 1992. Magnitude and geographic-variation of the radiocarbon content in Antarctic marine life - implications for reservoir corrections in radiocarbon dating. Quaternary Science Reviews 11, 697-708.

Graham, A.G.C., Larter, R.D., Gohl, K., Hillenbrand, C.-D., Smith, J.A., Kuhn, G., 2009. Bedform signature of a West Antarctic palaeo-ice stream reveals a multi-temporal record of flow and substrate control. Quaternary Science Reviews 28, 2774-2793. doi:10.1016/j.quascirev.2009.07.003.

Graham, A.G.C., Larter, R.D., Gohl, K., Dowdeswell, J.A., Hillenbrand, C.-D., Smith, J.A., Evans, J., Kuhn, G., 2010. Flow and retreat of the Late Quaternary Pine Island-Thwaites palaeo-ice stream, West Antarctica. Journal of Geophysical Research: Earth Surface 115, F03025, doi:10.1029/2009JF001482.

Hemer, M.A., Post, A.L., O’Brien, P.E., Craven, M., Truswell, E.M., Roberts, D., Harris, P., T., 2007. Sedimentological signatures of the sub-Amery Ice Shelf circulation. Antarctic Science 19, 497-506.

Heroy, D.C., Anderson, J.B., 2005. Ice-sheet extent of the Antarctic Peninsula region during the Last Glacial Maximum (LGM) – Insights from glacial geomorphology. Geological Society of America Bulletin 117, 1497–1512.

Heroy, D.C., Anderson, J.B., 2007. Radiocarbon constraints on Antarctic Peninsula Ice Sheet retreat following the Last Glacial Maximum (LGM). Quaternary Science Reviews 26, 3286–3297.

Heroy, D., Sjunneskog, C., Anderson, J.B., 2008. Holocene climate change in the Bransfield Basin, Antarctic Peninsula: evidence from sediment and diatom analysis. Antarctic Science 20, 69–87, DOI: 10.1017/S0954102007000788.

Hillenbrand, C.-D., Grobe, H., Diekmann, B., Kuhn, G., Fütterer, D., 2003. Distribution of clay minerals and proxies for productivity in surface sediments of the Bellingshausen and Amundsen Seas (West Antarctica): relation to modern environmental conditions. Marine Geology 193, 253–271.

Hillenbrand, C.-D., Baesler, A., Grobe, H,, 2005. The sedimentary record of the last glaciation in the western Bellingshausen Sea (West Antarctica): Implications for the interpretation of diamictons in a polar-marine setting. Marine Geology 216, 191– 204, doi:10.1016/j.margeo.2005.01.007.

Hillenbrand, C.-D., Ehrmann, W., Larter, R.D., Benetti, S., Dowdeswell, J.A., Ó Cofaigh, C., Graham, A.G.C., Grobe, H., 2009. Clay mineral provenance of sediments in the southern Bellingshausen Sea reveals drainage changes of the West Antarctic Ice Sheet during the Late Quaternary. Marine Geology 265, 1-18.

Hillenbrand, C.-D., Smith, J.A., Kuhn, G., Esper, O., Gersonde, R., Larter, R.D., Maher, B., Moreton, S.G., Shimmield., T,M., Korte, M., 2010a. Age assignment of diatomaceous ooze deposited in the western Amundsen Sea Embayment after the Last Glacial Maximum. Journal of Quaternary Science 25, 280–295, DOI: 10.1002/jqs.1308.

Hillenbrand, C.-D., Larter R.D., Dowdeswell, J.A., Ehrmann, W., Ó Cofaigh, C., Benetti, S**.,** Graham, A.G.C.**,** Grobe, H., 2010b.The sedimentary legacy of a palaeo-ice stream on the shelf of the southern Bellingshausen Sea: Clues to West Antarctic glacial history during the Late Quaternary. Quaternary Science Reviews, doi:10.1016/j.quascirev.2010.06.028.

Hughes, T., 1981. The weak underbelly of the West Antarctic Ice Sheet. Journal of Glaciology 27, 518-525.

Jenkins, A., Dutrieux, P., Jacobs, S.S., McPhail, S.D., Perrett, J.R., Webb, A.T., White, D., 2010. Observations beneath Pine Island Glacier in West Antarctica and implications for its retreat. Nature Geoscience 3, 468 – 472, doi:10.1038/ngeo890.

Katz, R.F., Worster, G., 2010. Stability of ice-sheet grounding lines. Proceedings of the Royal Society 466, 1597–1620, doi:10.1098/rspa.2009.0434.

Kilfeather, A.A., Ó Cofaigh, C., Lloyd, J.M., Dowdeswell, J.D., Sheng, X., Moreton, S.G., in press. Ice stream retreat and ice shelf history in Marguerite Trough, Antarctic Peninsula: sedimentological and foraminiferal signatures. Geological Society of America Bulletin, in press.

King, E.C., Hindmarsh, R.C.A., Stokes, C.R., 2009. Formation of mega-scale glacial lineations observed beneath a West Antarctic ice stream. Nature Geoscience 2, 585-596.

Larter, R.D., Vanneste, L.E., 1995. Relict subglacial deltas on the Antarctic Peninsula outer shelf. Geology 23, 33-36.

Larter, R.D., Gohl, K., Hillenbrand, C-D., Kuhn, G., Deen, T.J., Dietrich, R., Eagles, G., Johnson, J.S., Livermore, R.A., Nitsche, F.O., Pudsey, C.J., Schenke, H-W., Smith, J.A., Udintsev, G., Uenzelmann-Neben, G., 2007. West Antarctic Ice Sheet Change since the Last Glacial Period. EOS Transactions, American Geophysical Union, 88, 189-190.

Larter, R.D., Graham, A.G.C., Gohl, K., Kuhn, G., Hillenbrand, C.-D., Smith, J.A., Deen, T.J., Livermore, R.A., Schenke, H.-W., 2009. Subglacial bedforms reveal complex basal regime in a zone of paleo-ice stream convergence, Amundsen Sea Embayment, West Antarctica. Geology 37, 411–414.

Le Brocq, A.M., Payne, A.J., Vieli, A., 2010. An improved Antarctic dataset for high resolution numerical ice sheet models (ALBMAP v1). Earth System Science Data Discussion 3, 195–230, doi:10.5194/essdd-3-195-2010.

Li, B., Yoon, H.-I., Park, B.-K., 2000. Foraminiferal assemblages and $CaCO_3$ dissolution since the last deglaciation in the Maxwell Bay, King George Island, Antarctica: Marine Geology 169, 239-257.

Licht, K.J., 2004. Antarctica's contribution to eustatic sea level during meltwater pulse-1A. Sedimentary Geology 165, 343–353.

Licht, K.J., Andrews, J.T., 2002. The ^{14}C record of Late Pleistocene ice advance and retreat in the central Ross Sea, Antarctica. Arctic, Antarctic and Alpine Research 34, 324–333.

Licht, K.J., Jennings, A.E., Andrews, J.T., Williams, K.M., 1996. Chronology of late Wisconsin ice retreat from the western Ross Sea, Antarctica. Geology 24, 223– 226.

Licht, K.J., Cunningham, W.L., Andrews, J.T., Domack, E.W., Jennings, A.E., 1998. Establishing chronologies from acid-insoluble organic ^{14}C dates on Antarctic (Ross Sea) and Arctic (North Atlantic) marine sediments. Polar Research 17, 203-216.

Licht, K.J., Dunbar, N.W., Andrews, J.T., Jennings, A.E., 1999. Distinguishing subglacial till and glacial marine diamictons in the western Ross Sea, Antarctica:

implications for a Last Glacial Maximum grounding line. Geological Society of America Bulletin 111, 91-103.

Licht, K.J., Lederer, J.R., Swope, R.J., 2005. Provenance of LGM glacial till (sand fraction) across the Ross Embayment, Antarctica. Quaternary Science Reviews 24, 1499-1520.

Long, A.J., Roberts, D.H., 2003. Late Weichselian deglacial history of Disko Bugt, West Greenland, and the dynamics of the Jakobshavns Isbrae ice stream. Boreas 32, 208-226.

Lowe, A.L., Anderson, J.B., 2002. Reconstruction of the West Antarctic ice sheet in Pine Island Bay during the Last Glacial maximum and its subsequent retreat history. Quaternary Science Reviews 21, 1879–1897.

Lowe, D.R., 1982. Sediment gravity flows: II - depositional models with special reference to the deposits of high density turbidity currents. Journal of Sedimentary Petrology 41, 168-186.

McKay, R.M., Dunbar, G.B., Naish, T., Barrett, P.J., Carter, L., Harper, M., 2008. Retreat history of the Ross Ice Sheet (Shelf) since the Last Glacial Maximum from deep-basin sediment cores around Ross Island. Palaeogeography, Palaeoclimatology, Palaeoecology 260, 145-261.

Mosola, A.B., Anderson, J.B., 2006. Expansion and rapid retreat of the West Antarctic Ice Sheet in Eastern Ross Sea: possible consequence of over extended ice streams? Quaternary Science Reviews 25 2177-2196.

Nitsche, F.O., Jacobs, S.S., Larter, R.D., Gohl, K., 2007. Bathymetry of the Amundsen Sea Continental Shelf: Implications for Geology, Oceanography, and Glaciology. Geochemistry, Geophysics, Geosystems 8, Q10009, doi:10.1029/2007GC001694.

Ó Cofaigh, C., Dowdeswell, J.A., Allen, C.S., Hiemstra, J., Pudsey, C.J., Evans, J., Evans, D.J.A., 2005. Flow dynamics and till genesis associated with a marine-based Antarctic palaeo-ice stream. Quaternary Science Reviews 24, 709e740.

Ó Cofaigh, C., Evans, J., Dowdeswell, J.A., Larter, R.D., 2007. Till characteristics, genesis and transport beneath Antarctic paleo-ice streams. Journal of Geophysical Research 112, F03006.

Ohkouchi, N., Eglinton, T.I., 2006. Radiocarbon constraint on relict organic carbon contributions to Ross Sea sediments. Geochemistry, Geophysics, Geosystems 7, Q04012.

Ohkouchi, N., Eglinton, T.I., 2008. Compound-specific radiocarbon dating of Ross Sea sediments: a prospect for constructing chronologies in high-latitude oceanic sediments. Quaternary Geochronology 3, 235–243.

Payne, A. J., Vieli, A., Shepherd, A.P., Wingham, D.J., Rignot, E., 2004. Recent dramatic thinning of largest West Antarctic ice stream triggered by oceans. Geophysical Research Letters 31, L23401, doi:10.1029/2004GL021284.

Payne, A.J., Holland, P.R., Shepherd, A., Rutt., I.C., Jenkins, A., Joughin, I., 2007. Numerical modeling of ocean-ice interactions under Pine Island Bay's ice shelf', Journal of Geophysical Research 112, 1-14, DOI: 10.1029/2006JC003733.

Petschick, R., Kuhn, G., Gingele, F.X., 1996. Clay mineral distribution in surface sediments of the South Atlantic: sources, transport, and relation to oceanography. Marine Geology 130, 203-229.

Pritchard, H.D., Arthern, R.J., Vaughan, D.G., Edwards, L.A., 2009. Extensive dynamic thinning on the margins of the Greenland and Antarctic ice sheets. Nature 61, 971-975, doi:10.1038/nature08471.

Pudsey, C.J., Murray, J.W., Appleby, P. & Evans, J., 2006. Ice shelf history from petrographic and foraminiferal evidence, Northeast Antarctic Peninsula. Quaternary Science Reviews 25, 2357-2379.

Rignot, E., 1998. Fast recession of a West Antarctic glacier, Science 281, 549– 551.

Rignot, E., 2006. Changes in ice dynamics and mass balance of the Antarctic ice sheet. Philosophical Transaction of the Royal Society, doi:10.1098/rsta.2006.1793.

Rosenheim, B.E., Day, M.B., Domack, E., Schrum, H., Benthien, A., Hays, J.M., 2008. Antarctic sediment chronology by programmed-temperature pyrolysis: methodology and data treatment. Geochemistry, Geophysics, Geosystems 9, Q04005. doi:10.1029/2007GC001816.

Schoof, C., 2007. Ice sheet grounding line dynamics: Steady states, stability and hysteresis. Journal of Geophysical Research 112, F03S28, doi:10.1029/2006JF000664.

Scott, J.B.T., Gudmundsson, G.H., Smith, A.M., Bingham, R.G., Pritchard, H.D., Vaughan, D.G., 2009. Increased rate of acceleration on Pine Island Glacier strongly coupled to changes in gravitational driving stress. The Cryosphere 3, 125–131.

Shepherd, A., Wingham, D., Rignot, E., 2004. Warm ocean is eroding West Antarctic Ice Sheet. Geophysical Research Letters 31, L23402.

Shepherd, A., Wingham, D., Wallis, D., Giles, K., Laxon, S., Sundal, A. V., 2010 Recent loss of floating ice and the consequent sea level contribution. Geophysical Research Letters 37, L13503, doi:10.1029/2010GL042496.

Shipp, S.S., Anderson, J.B., Domack, E.W., 1999. Late Pleistocene–Holocene retreat of the West Antarctic ice-sheet system in the Ross Sea: a new perspective: Part 1. Geophysical results. Geological Society of America Bulletin 111, 1486– 1516.

Smith, J.A., Hillenbrand, C.-D., Larter, R.D., Graham, A.G.C., Kuhn, G., 2009. The sediment infill of subglacial meltwater channels on the West Antarctic continental shelf. Quaternary Research 71, 190–200.

Stuiver, M., Reimer, P.J, Reimer, R.W., 2005. CALIB 5.0 (http://calib.qub.ac.uk/calib/manual/).

Thoma, M., Jenkins, A.,Holland, D., Jacobs, S.S., 2008. Modelling Circumpolar Deep Water intrusions on the Amundsen Sea continental shelf, Antarctica. Geophysical Research Letters 35, L18602, doi:10.1029/2008GL034939.

Thomas, R., Stephenson, S., Bindschadler , R., Shabtaie, S., Bentley, C., 1988. Thinning and grounding-line retreat on Ross Ice Shelf, Antarctica. Annals of Glaciology 11, 165–172.

Vaughan, D.G., 2008. West Antarctic Ice Sheet collapse – the fall and rise of a paradigm. Climatic Change 91 65-79, DOI10.1007/s10584-008-9448-3.

Vaughan, D.G., Arthern, R., 2007. Why Is It Hard to Predict the Future of Ice Sheets? Science 315, 1503–1504. doi: 10.1126/science.1141111.

Vaughan, D. G., Corr, H.F.J., Ferraccioli, F., Frearson, N., O'Hare, A., Mach, D., Holt, J.W., Blankenship, D.D., Morse, D.L., Young, D.A., 2006. New boundary conditions for the West Antarctic ice sheet: Subglacial topography beneath Pine

Island Glacier. Geophysical Research Letters 33, L09501, doi:10.1029/2005GL025588.

Verleyen, E., Hodgson, D.A., Milne, G.A., Sabbe, K., Vyverman, W., 2005. Relative sea-level history from the Lambert glacier region, East Antarctica, and its relation to deglaciation and Holocene glacier readvance. Quaternary Research 63, 45–52.

Villinski, J.C., Hayes, J.M., Brassell, S.C., Riggert, V.L., Dunbar, R.B., 2008. Sedimentary sterols as biogeochemical indicators in the Southern Ocean. Organic Geochemistry 39, 567–588.

Walker, D. P., Brandon, M.A., Jenkins, A., Allen, J.T., Dowdeswell, J.A., Evans, J., 2007. Oceanic heat transport onto the Amundsen Sea shelf through a submarine glacial trough. Geophysical Research Letters 34, L02602, doi:10.1029/2006GL028154.

Yokoyama, Y., Lambeck, K., de Dekhar, P., Johnston, P., Fifield, L.K., 2000. Timing of last glacial maximum from observed sea level minima. Nature 406, 713–716

11. Table and Figure captions

Table 1. Site information on sediment cores from the western Amundsen Sea. VC= vibrocore; BC= boxcore; GBC=giant boxcore; GC=gravity core.

Table 2. Uncorrected, corrected and calibrated AMS ^{14}C dates from the western Amundsen Sea together with locations, sample depth and dated material (AIO= acid-insoluble organic matter). †Reservoir correction: For carbonate samples we use the accepted marine reservoir correction of 1,300 years (Berkman and Forman, 1996) and our AIO ages were corrected by subtracting core-top ages. We show the entire 1σ range for each calibrated age (Min, Max), but quote the mean age throughout the text. *Sample used for downcore correction because of insufficient surface material available/surface missing. **Denotes calibration using Fairbanks calibration curve (http://radiocarbon.ldeo.columbia.edu/research/radcarbcal.htm) for samples older than 25,000 ^{14}C yr BP (Fairbanks et al., 2005).

Table 3. Time slices for deglaciation of the western Amundsen Sea (calibrated ^{14}C years) providing an upper and lower estimate for the minimum age for ice retreat. Numbered points refer to the dashed lines displayed in Fig. 5d. Ages are rounded to the nearest 50 years.

Figure 1. Map of the Amundsen Sea showing locations of sediment cores and surface sediment samples (note: at sites where both box cores and long cores were recovered, only the IDs of the vibrocores (VC) and gravity cores (PS cores) are shown. For a summary of all locations see Table 1) and regional bathymetry (Nitsche et al., 2007). Sediment cores were recovered along transects in the three tributary troughs (Dotson, Getz A and Getz B represented by solid, dashed and dotted lines respectively). (b) Location of Amundsen Sea (AS) and other places referred to in text, BS=Bellingshausen Sea, MB=Marguerite Bay. Inset (c) shows detailed bathymetry of the inner shelf area (Larter et al., 2009).

Figure 2. Representative core logs and core data from the western Amundsen Sea, showing simplified lithology, shear strength (green line, closed black circles), water content (blue line, open triangles), magnetic susceptibility (measured with the MSCL; red line), contents of mud (0-63 µm; white fill), sand (63 µm-2 mm; grey fill) and gravel (>2 mm; black fill), organic carbon (C_{org}) (blue line, open triangles), C/N (black line, closed circles), clay mineral data (smectite/chlorite ratio) and $CaCO_3$ data (orange line, open squares). Uncorrected (black circle) and calibrated (red circle) ^{14}C ages are also shown (with the deglacial age highlighted in orange) together with a facies log. Crossed circles represent foraminiferal ^{14}C ages. *Where more than one age from a core meets our criteria (e.g., the ooze ages from PS69/274-1 and VC424), the oldest age is selected as the age for deglaciation. (a) Shows the ideal stratigraphic succession for dating the deglaciation (consisting of Facies 1-3) and Facies 1 and 2 (b). (c) We also incorporated additional stratigraphies, such as iceberg turbates (Facies 4) but exclude others from our deglacial model, either because of its unsuitable depositional facies (here gravity-flow deposit; Facies 5 (d)) or that the ^{14}C ages did not meet our criteria.

Figure 3. Map of uncorrected surface ^{14}C ages (AIO: regular font; foraminifera: italics) from the western Amundsen Sea shelf. The map of surface ages illustrates the problems of fossil carbon contamination of surface sediments in this area.

Figure 4. (a) All downcore ^{14}C ages (calibrated) plotted against distance from the grounding line (GL). Closed circles represent the most reliable dates, based on the selection criteria outlined in section 2.1 and 2.2), whilst open circles of the same

colour represent all other ages from each particular core. (b) Most reliable ^{14}C (calibrated) dates plotted against distance from the modern GL. Crossed circles represent foraminiferal ^{14}C ages.

Figure 5. Retreat profiles for the (a) Dotson, (b) Getz A and (c) Getz B tributary troughs plotted against distance from the modern grounding line (GL). In each figure, the solid line represents our favoured model for deglaciation, whilst the full age range (grey shaded cell) for deglaciation of the inner shelf, with clear minimum and maximum ages for deglaciation , is shown in (d) (cf. ages listed in Table 2). The numbers on Fig. 5d refer to the time slices presented in Table 3.

Figure 6. Comparison of the retreat history in the western Amundsen Sea (red lines [online version only], black crosses), Marguerite Bay (black dot-dash line, open circles; Heroy and Anderson, 2005; 2007; Kilfeather et al., in press), western Ross Sea (dashed black line, open triangles; Licht et al., 1996; Domack et al., 1999; Licht and Andrews, 2002; McKay et al., 2008) and Getz D trough (grey diamonds; Anderson et al., 2002). For the western ASE, the red dotted line represents the minimum and maximum ages for deglaciation, whilst the dashed red line gives the mean (values from Table 3). Calibrated ages are plotted against distances from the modern grounding line (GL), which have been normalised using the distance between the GL and shelf edge for each trough/shelf sector. Grey vertical bars show timing of global meltwater pulses; mwp1a, mwp1b, 19 ka mwp (Fairbanks et al., 1989; Yokohama et al., 2000; Clark et al., 2002).

Figure 7. Retreat trajectory for the deglaciation of the WAIS in the western Amundsen Sea. Calculated average retreat rates are shown together with the trajectory of modern and palaeo retreat rates (numbered lines, bottom left panel) for Ice Stream B and C (Conway et al., 1999), Pine Island Glacier (Rignot, 1998; Scott et al., 2009) and Bellingshausen Sea (Hillenbrand et al., 2010b). Retreat rates are calculated from the deglacial profiles shown in Figure 5. Grey shading represents our deglacial envelope for the mid-inner shelf.

Figure 8. Along trough profiles and core locations for the Dotson (a), Getz A (b) and Getz B (c) tributary troughs. Dashed line shows calculated retreat rates derived from the deglacial profiles or 'retreat trajectories' shown in Fig. 5a-c, and shown here as the grey dotted lines. For the Getz B trough and mean ooze age (cores PS69/274-1, 275-1 and 273-2) was used to calculate the retreat rate for the mid-shelf. Trough profiles were extracted from a combined multibeam (50 m) and regional (3 km) bathymetric grid (Nitsche et al., 2007).

12. Supplementary Tables and Figures

Table 1. Parameters measured for each core.

Supplementary Figure 1a-q: Core logs and data from the western Amundsen Sea, showing simplified lithology, shear strength (green line, closed black circles), water content (blue line, open triangles), magnetic susceptibility (measured with the MSCL) (red line), contents of mud (0-63 µm; white fill), sand (63 µm -2 mm; grey fill) and gravel (>2 mm; black fill), organic carbon (C_{org}) (blue line, open triangles), C_{org}/N_{tot}

(black line, closed circles), clay mineral data (smectite/chlorite ratio) and $CaCO_3$ data (orange line, open squares) . Uncorrected (black circle) and calibrated (red circle) ^{14}C ages are also shown with the deglacial age highlighted in orange. Crossed circles represent foraminiferal ^{14}C ages. Where more than one age from a core meets our criteria (e.g., the ooze ages from VC424), the oldest age is selected as the age for deglaciation.

Table 1

Table 1.

Cruise	Gear	Core	Latitude (°S)	Longitude (°W)	Water depth (m)	Core Recovery (m)
JR141	VC	VC408	-73.7951	-112.8176	787	3.68
JR141	BC	BC409	-73.7951	-112.8175	787	0.40
JR141	BC	BC412	-73.9229	-115.8570	1128	0.46
JR141	VC	VC415	-73.8958	-115.9311	918	4.34
JR141	BC	BC416	-74.1361	-112.4514	893	0.28
JR141	VC	VC417	-74.1361	-112.4514	891	1.73
JR141	VC	VC419	-74.1416	-112.8564	806	4.80
JR141	BC	BC420	-74.1416	-112.8566	806	0.37
JR141	BC	BC421	-73.6179	-113.7093	833	0.48
JR141	VC	VC422	-73.6179	-113.7093	833	5.76
JR141	BC	BC423	-73.4471	-115.1980	1073	0.41
JR141	VC	VC424	-73.4469	-115.1981	1073	5.37
JR141	VC	VC425	-73.7029	-115.4860	1020	5.09
JR141	VC	VC428	-73.1425	-115.7044	758	4.95
JR141	BC	BC429	-73.1417	-115.7030	765	0.41
JR141	VC	VC430	-72.3045	-118.1637	512	4.52
JR141	BC	BC431	-72.3046	-118.1638	512	0.14
JR141	VC	BC435	-71.8165	-117.4300	466	0.11
JR141	BC	VC436	-71.8136	-117.4335	466	5.97
ANT-XXIII/4	GC	PS69/259-1	-74.3017	-110.2653	258	3.06
ANT-XXIII/4	GC	PS69/265-3	-73.6688	-113.0385	692	1.29
ANT-XXIII/4	GC	PS69/267-1	-73.3952	-114.5592	863	2.97
ANT-XXIII/4	GBC	PS69/267-2	-73.3952	-114.5652	864	ca. 0.3
ANT-XXIII/4	GC	PS69/272-2	-73.8927	-118.4865	1578	1.57
ANT-XXIII/4	GBC	PS69/272-3	-73.8920	-118.4782	1576	0.32
ANT-XXIII/4	GC	PS69/273-2	-73.9617	-117.8432	1352	3.29
ANT-XXIII/4	GC	PS69/274-1	-73.8560	-117.7757	1452	4.53
ANT-XXIII/4	GC	PS69/275-1	-73.8888	-117.5483	1518	4.79
ANT-XXIII/4	GBC	PS69/275-2	-73.8887	-117.5483	1517	0.27
ANT-XXIII/4	GC	PS69/280-1	-73.9358	-111.6235	625	1.42
ANT-XXIII/4	GBC	PS69/283-5	-72.7643	-115.3770	612	0.34

Table 2

Table 2.

Core	Publication Code	Core location Lat.	Long.	Core Depth (cmbsf)	Material Dated	Uncorrected ^{14}C Age (yrs BP)	±1σ	Reservoir correction†	Corrected ^{14}C age (yr BP)	Calibrated Age (yr BP)	±1s Min	Max
BC409	SUERC-20891	-73.7951	-112.8175	Surface	AIOM	5135	38	N/A	0	0	-	-
VC408	SUERC-20890	-73.7951	-112.8176	88	AIOM	14692	62	5135	9557	10777.5	10478	11077
VC408	SUERC-20889	-73.7951	-112.8176	108	AIOM	14646	63	5135	9511	10879	10689	11069
BC410	SUERC-22286	-73.5669	-116.8459	Surface	AIOM	3262	37	N/A	N/A	0	-	-
VC411	SUERC-22269	-73.5670	-116.8459	15	AIOM	5945	35	3262	2683	2801.5	2753	2850
VC411	SUERC-22270	-73.5670	-116.8459	109	AIOM	35373	785	3262	32111	37498**	-	-
VC411	SUERC-22271	-73.5670	-116.8459	185	AIOM	34715	728	3262	31453	36831**	-	-
BC412	SUERC-10892	-73.9229	-115.8570	Surface	AIOM	4723	35	N/A	0	0	-	-
VC415	SUERC-26014	-73.8958	-115.9311	1	AIOM	4860	36	N/A	0	0	-	-
VC415	SUERC-20892	-73.8958	-115.9311	78	AIOM	11730	48	4723	7007	7860	7792	7928
VC415	SUERC-26015	-73.8958	-115.9311	91	AIOM	13105	55	4723	8382	9394.5	9312	9477
VC415	SUERC-11805	-73.8958	-115.9311	93	AIOM	13677	57	4723	8954	10071.5	9936	10207
VC415	SUERC-26018	-73.8958	-115.9311	159	AIOM	37223	987	4723	32500	37886**	-	-
BC416	SUERC-10893	-74.1361	-112.4514	Surface	AIOM	6405	35	N/A	0	0	-	-
VC417	SUERC-20893	-74.1361	-112.4514	38	AIOM	12741	53	6405	6336	7247	7175	7319
VC417	SUERC-26012	-74.1361	-112.4514	47	AIOM	13208	55	6405	6803	7635.5	7594	7677
VC417	SUERC-13343	-74.1361	-112.4514	75	AIOM	15333	47	6405	8928	10059.5	9934	10185
VC417	SUERC-20896	-74.1361	-112.4514	85	AIOM	16092	72	6405	9687	11051.5	10870	11233
VC417	SUERC-26013	-74.1361	-112.4514	90	AIOM	16307	76	6405	9902	11454.5	11215	11694
VC418	SUERC-22272	-73.9706	-112.2208	39	AIOM	10480	46	5135	5345	6110.5	6013	6208
VC418	SUERC-22275	-73.9706	-112.2208	51	AIOM	11469	47	5135	6334	7246.5	7177	7316
BC420	SUERC-21437	-74.1416	-112.8566	Surface	AIOM	6429	36	N/A	0	0	-	-
VC419	SUERC-14120	-74.1416	-112.8564	384	Mixed benthic	11237	40	1300	9937	11431.5	11261	11602
BC421	SUERC-13337	-73.6179	-113.7093	Surface	AIOM	5291	35	N/A	0	0	-	-
VC422	SUERC-11801	-73.6179	-113.7093	165	AIOM	19991	117	5291	14700	17792.5	17551	18034
VC422	SUERC-14424	-73.6179	-113.7093	486	AIOM	28495	334	5291	23204	27838**	-	-
BC423	SUERC-13338	-73.4471	-115.1980	Surface	AIOM	4289	35	N/A	0	0	-	-
VC424	SUERC-14426	-73.4469	-115.1981	84	AIOM	8108	40	4289	3819	4217	4150	4284
VC424	SUERC-21453	-73.4469	-115.1981	205	AIOM (ooze)	12183	51	1300	10883	12869	12801	12937
VC424	SUERC-11800	-73.4469	-115.1981	266	AIOM (ooze)	11803	48	1300	10503	12479	12277	12681
VC424	SUERC-21456	-73.4469	-115.1981	276.5	AIOM (ooze)	13517	56	1300	12217	14119	14005	14233
VC425	SUERC-14423	-73.7029	-115.4860	221	AIOM (ooze)	12868	54	1300	11568	13411	13287	13535
BC426	SUERC-22287	-73.6691	-114.9782	Surface	AIOM	3389	37	N/A	0	0	-	-
VC427	SUERC-22276	-73.6689	-114.9780	179	AIOM (ooze)	12139	55	1300	10839	12862	12820	12904
VC427	SUERC-22277	-73.6689	-114.9780	395	AIOM	14159	63	1300	12859	15258	15038	15478
VC427	SUERC-22278	-73.6689	-114.9780	398	AIOM	17164	82	3389	13775	16400	16187	16613
BC429	SUERC-10894	-73.1417	-115.7030	Surface	AIOM	3865	35	N./A	0	0	-	-
VC428	SUERC-21438	-73.1425	-115.7044	38	AIOM	8448	41	3865	4583	5261.5	5080	5443
VC428	SUERC-21439	-73.1425	-115.7044	65	AIOM	10384	45	3865	6519	7410.5	7337	7484
VC428	SUERC-11806	-73.1425	-115.7044	91	AIOM	15841	72	3865	11976	13837	13759	13915
BC431	SUERC-18332	-72.3046	-118.1638	Surface	N.pach	1693	37	1300	393	419.5	334	505
BC431	SUERC-25665	-72.3046	-118.1638	13	N.pach/Benthic	4919	25	1300	3619	3976	3894	4058
VC430	SUERC-14788	-72.3045	-118.1637	5	AIOM	9010	42	-	-	-	-	-
VC430	SUERC-14789	-72.3045	-118.1637	240	Benthic/N.pach	10979	40	1300	9679	11055.5	10903	11208
VC430	SUERC-26719	-72.3045	-118.1637	380	Benthic/N.pach	10784	39	1300	9484	10833	10609	11057
BC435	SUERC-11807	-71.8165	-117.4300	Surface	N.pach	2768	35	1300	1468	1349.5	1318	1381
BC435	SUERC-10895	-71.8165	-117.4300	Surface	AIOM	5134	35	N/A	0	0	-	-
VC436	SUERC-22265	-71.8136	-117.4335	60	Benthic/N.pach	20115	71	1300	18815	22350.5	22244	22457
VC436	SUERC-23808	-71.8136	-117.4335	61	Benthic/N.pach	18080	52	1300	16780	19944.5	19819	20070
VC436	SUERC-22266	-71.8136	-117.4335	160	N.pach	9941	39	1300	8641	9731	9565	9897
VC436	SUERC-21440	-71.8136	-117.4335	240	AIOM	34518	705	5134	29384	34788**	-	-
VC436	SUERC-14118	-71.8136	-117.4335	240	N.pach	10220	39	1300	8920	10118.5	9958	10279
VC436	SUERC-21441	-71.8136	-117.4335	400	AIOM	27388	292	5134	22254	26757**	-	-
VC436	SUERC-14119	-71.8136	-117.4335	400	N.pach	12181	42	1300	10881	12867	12803	12931
VC436	SUERC-22267	-71.8136	-117.4335	540	Benthic/N.pach	14975	46	1300	13675	16266.5	16036	16497
PS69/265-3	SUERC-18630	-73.6688	-113.039	3*	AIOM	4403	36	N/A	0	0	-	-
PS69/265-3	SUERC-18631	-73.6688	-113.039	44	AIOM	11315	46	4403	6912	7737	7688	7786
PS69/267-2	SUERC-18632	-73.3952	-114.565	3*	AIOM	4124	38	N/A	0	0	-	-
PS69/267-2	SUERC-21442	-73.3952	-114.565	40	AIOM	10371	44	4124	6247	7143.5	7031	7256
PS69/267-2	SUERC-18633	-73.3952	-114.565	72	AIOM	15108	66	4124	10984	12912.5	12863	12962
PS69/272-3	SUERC-11791	-73.892	-118.478	Surface	AIOM	5048	35	N/A	0	0	-	-
PS69/273-2	SUERC-13342	-73.9617	-117.843	192	AIOM (ooze)	11945	38	1300	10645	12610	12400	12820
PS69/274-1	SUERC-14428	-73.856	-117.776	60	AIOM	7740	39	3950	3790	4221	4094	4348
PS69/274-1	SUERC-14429	-73.856	-117.776	140	AIOM	14199	61	3950	10249	12089	11826	12352
PS69/274-1	SUERC-21448	-73.856	-117.776	177	AIOM	14821	64	3950	10871	12879.5	12828	12931
PS69/274-1	SUERC-15252	-73.856	-117.776	210	AIOM (ooze)	12034	69	1300	10734	12757	12645	12869
PS69/274-1	SUERC-11798	-73.856	-117.776	232	AIOM (ooze)	11967	49	1300	10667	12618	12405	12831
PS69/274-1	SUERC-21449	-73.856	-117.776	312	AIOM	24416	198	3950	20466	24768.5	24210	25327
PS69/275-2	SUERC-13341	-73.8887	-117.548	Surface	AIOM	3950	35	N/A	0	0	0	0
PS69/275-1	SUERC-21450	-73.8888	-117.548	53	AIOM	8795	42	3950	4845	5571	5486	5656
PS69/275-1	SUERC-14427	-73.8888	-117.548	108	AIOM	13154	56	3950	9204	10387.5	10265	10510
PS69/275-1	SUERC-11799	-73.8888	-117.548	204	AIOM (ooze)	11543	47	1300	10243	11955.5	11716	12195
PS69/275-1	SUERC-21451	-73.8888	-117.548	228.5	AIOM	15703	69	3950	11753	13632	13504	13760
PS69/275-1	SUERC-21452	-73.8888	-117.548	430	AIOM	28020	311	3950	24070	28814**	-	-
PS69/280-1	SUERC-18636	-73.9358	-111.624	6*	AIOM	7019	38	N/A	0	0	-	-
PS69/280-1	SUERC-21443	-73.9358	-111.624	20	AIOM	17021	80	7019	10002	11503	11312	11694
PS69/280-1	SUERC-18637	-73.9358	-111.624	25	AIOM	28247	321	7019	21228	25528	25056	26000
PS69/283-5	SUERC-11792	-72.7643	-115.377	Surface	AIOM	5076	35	N/A	0	0	-	-
PS69/283-5	SUERC-20886	-72.7643	-115.377	22	AIOM	9536	42	5076	4977	5285.5	5276	5295
PS69/285-5	SUERC-21446	-72.7643	-115.377	10	AIOM	4556	36	5076	5076	-	-	-

Table 3

Table 3.

Map # (Fig. 5d)	Latitude (°S)	Longitude (°W)	Deglacial age (cal. yr BP)			Shelf location
			min	max	mean	
1	-71.8136	-117.4335	-	22350	22350	Outer shelf
2	-73.1425	-115.7044	13850	-	13850	Mid-shelf
3	-73.2371	114.3391	12900	13750	13325	Mid-shelf
4	-73.4469	-115.1981	12500	13550	13025	Mid-shelf
5	-73.6689	-114.9780	11600	13450	12525	Mid-shelf
6	-73.7029	-115.4860	11500	13400	12450	Mid-shelf
7	-73.856	-117.776	11450	12900	12175	Inner-shelf
8	-73.962	-117.843	11200	12600	11900	Inner-shelf
9	-73.8958	-115.9311	10072	-	10072	Inner-shelf

Figure 1

Figure 1.

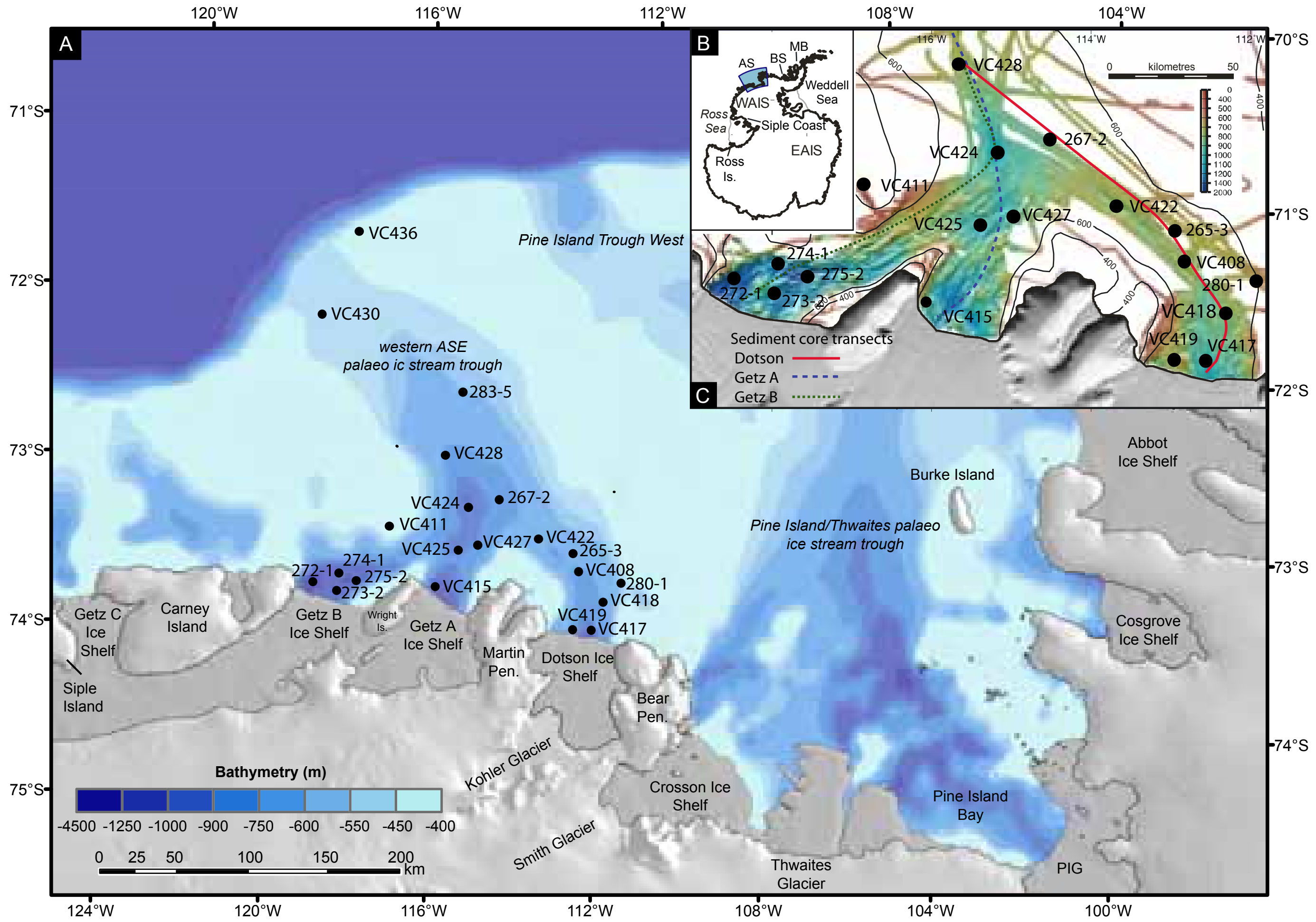

Figure 2_pt1

Figure 2a-c.

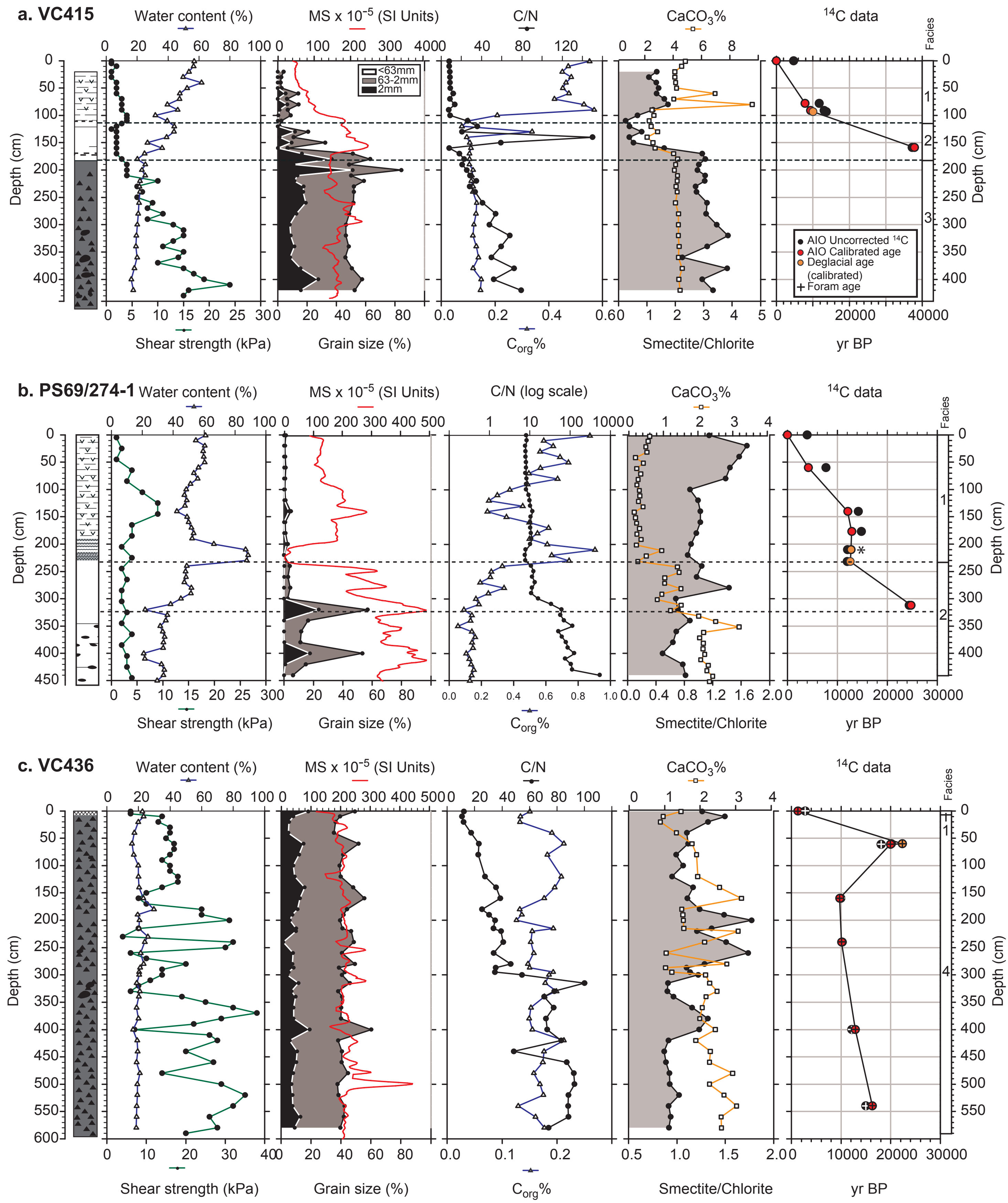

Figure 2_pt2

Figure 2d.

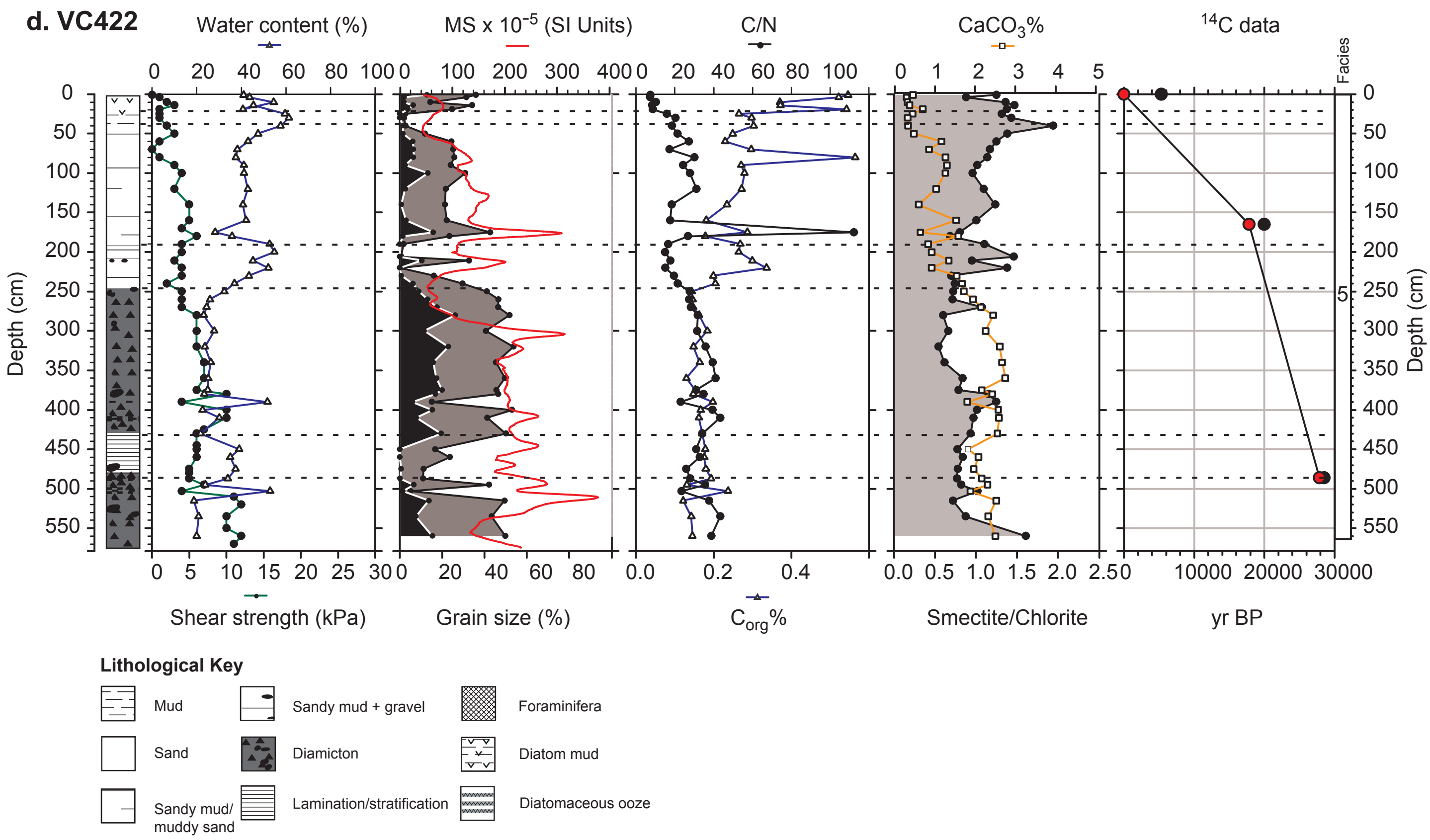

Figure 3

Figure 3.

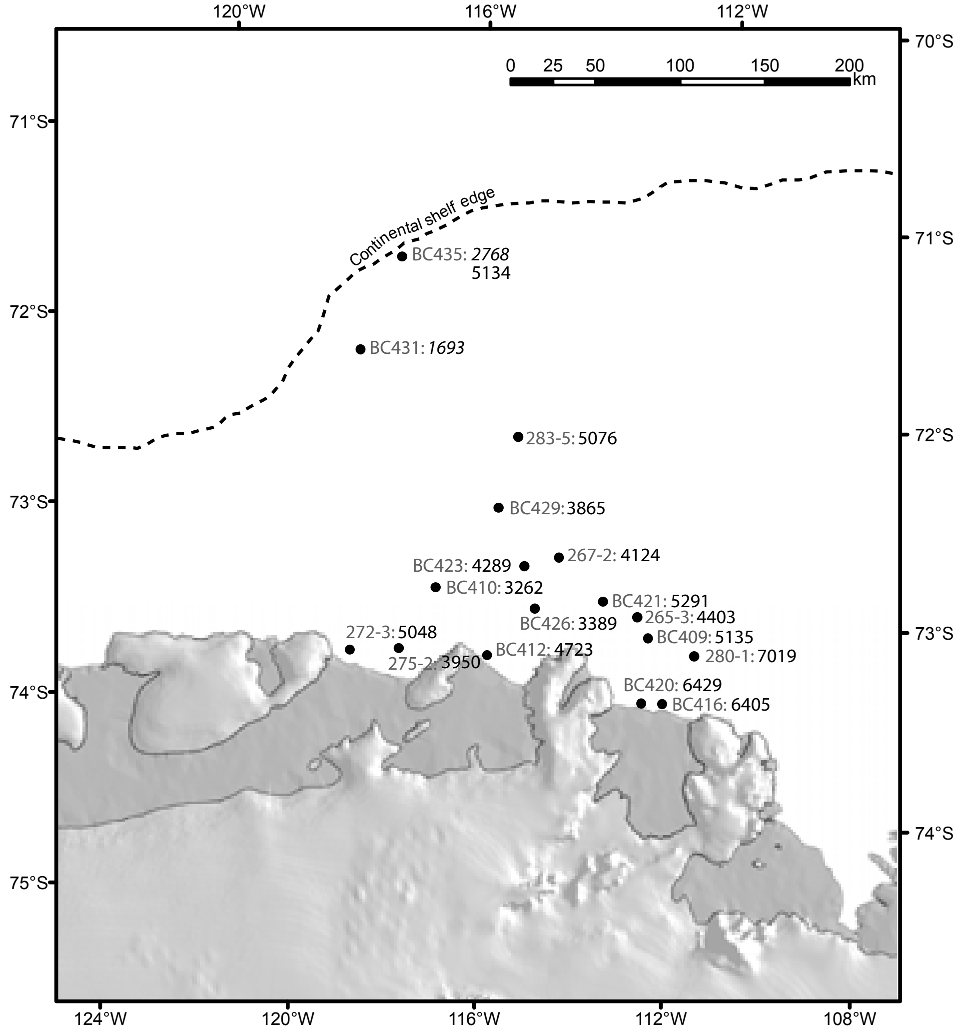

Figure 4

Figure 4.

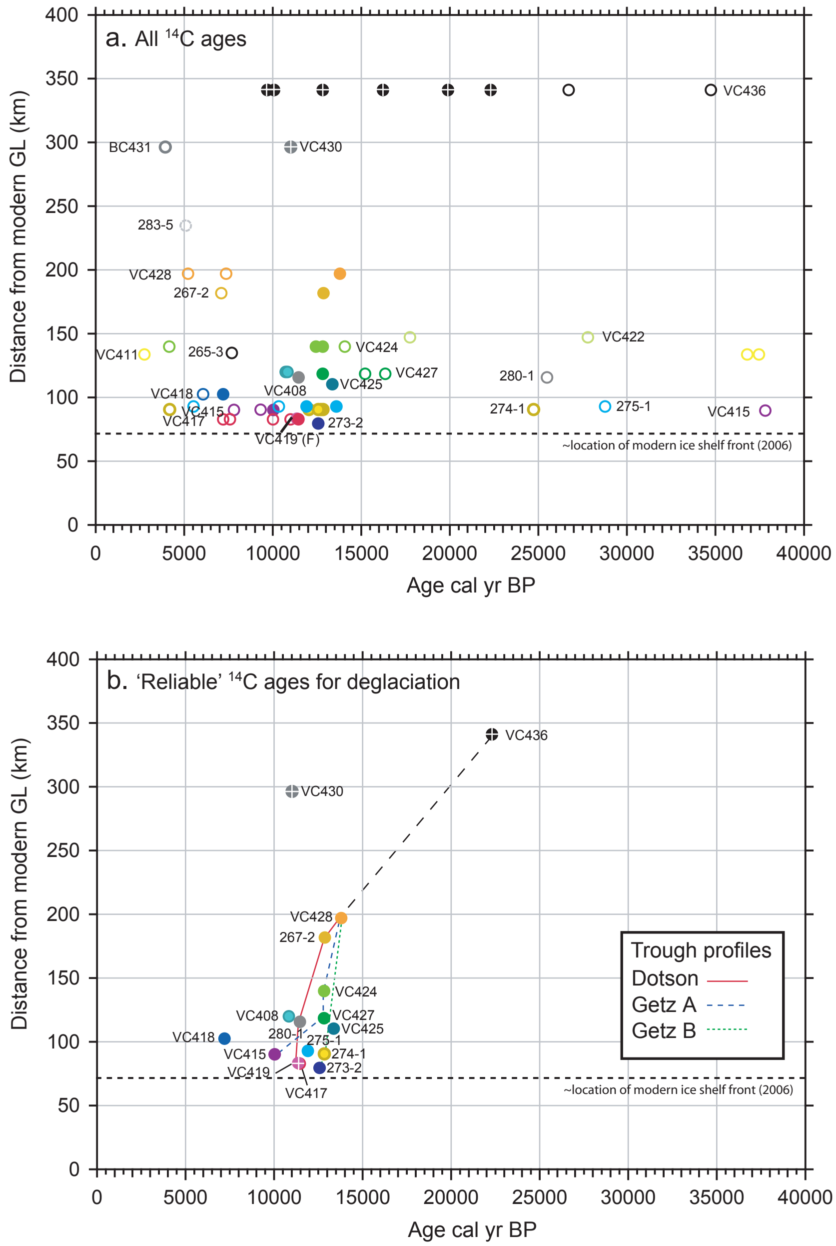

Figure 5

Figure 5.

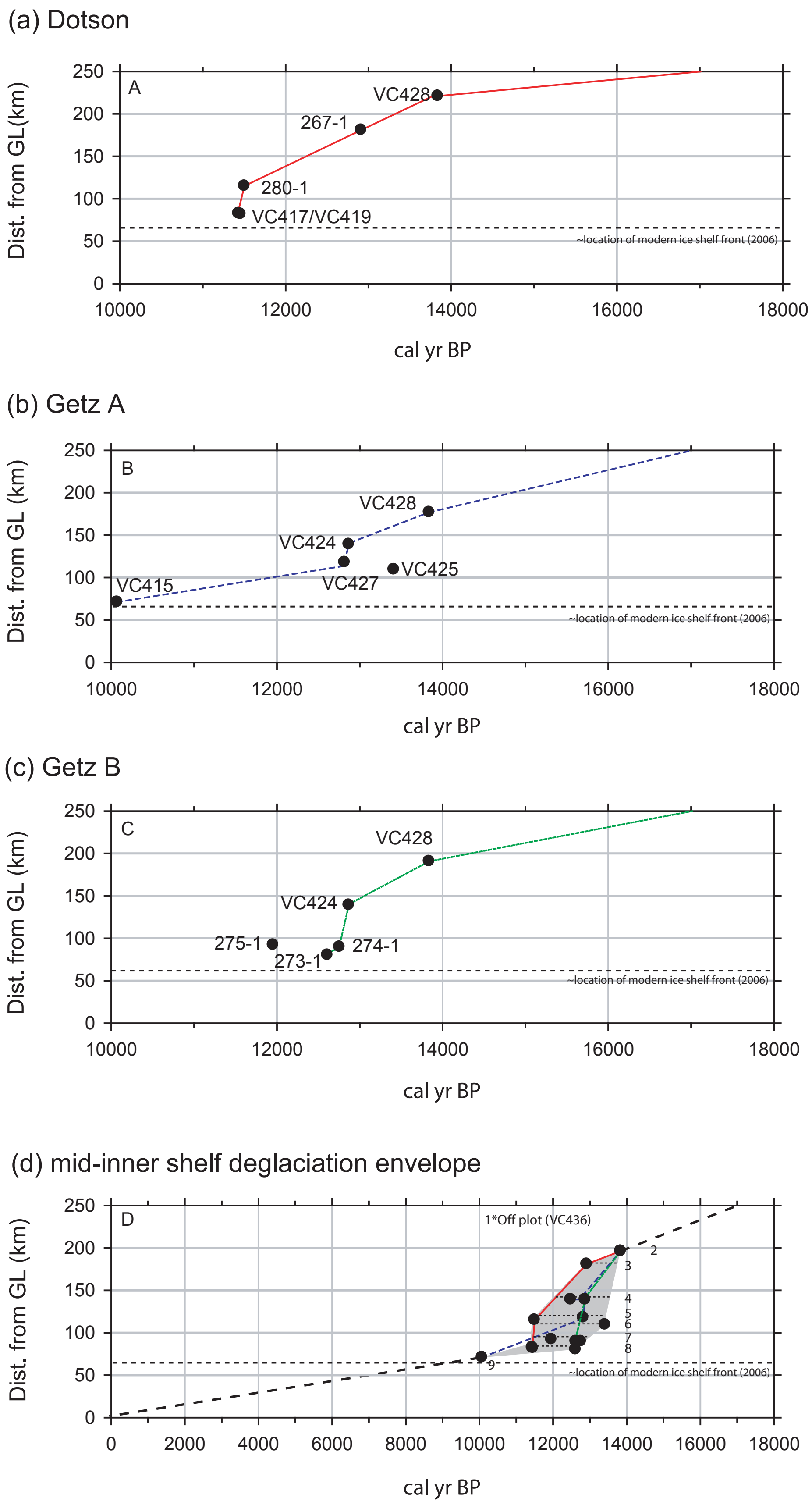

Figure 6

Figure 6.

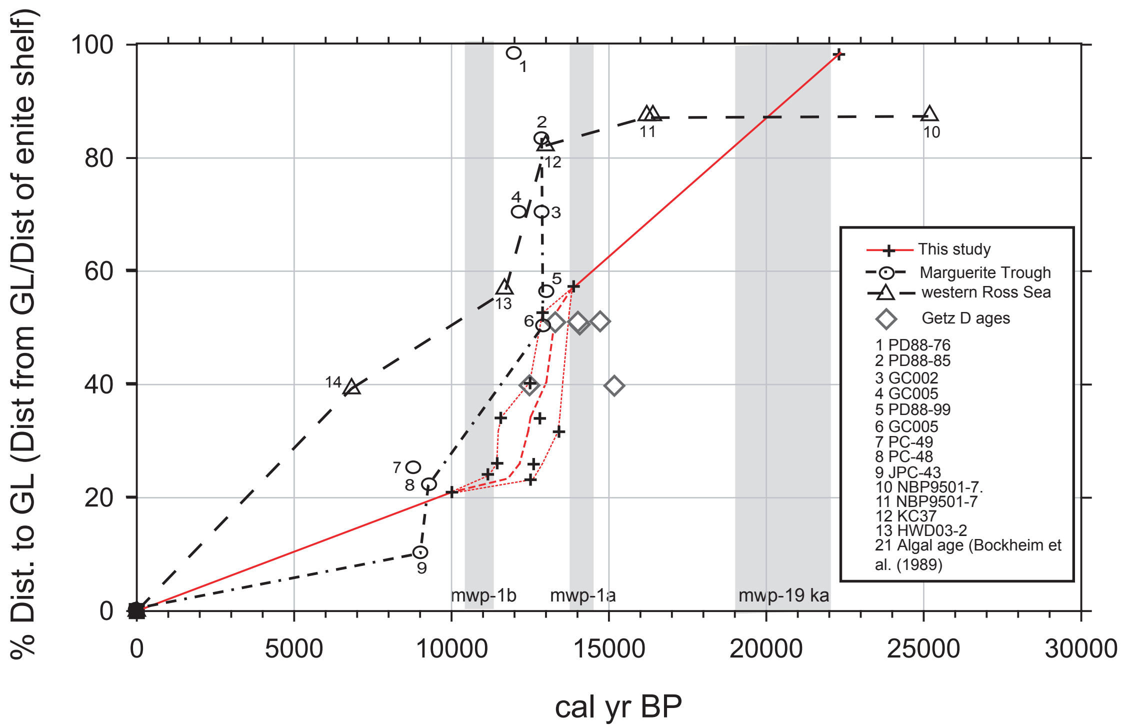

Figure 7

Figure 7.

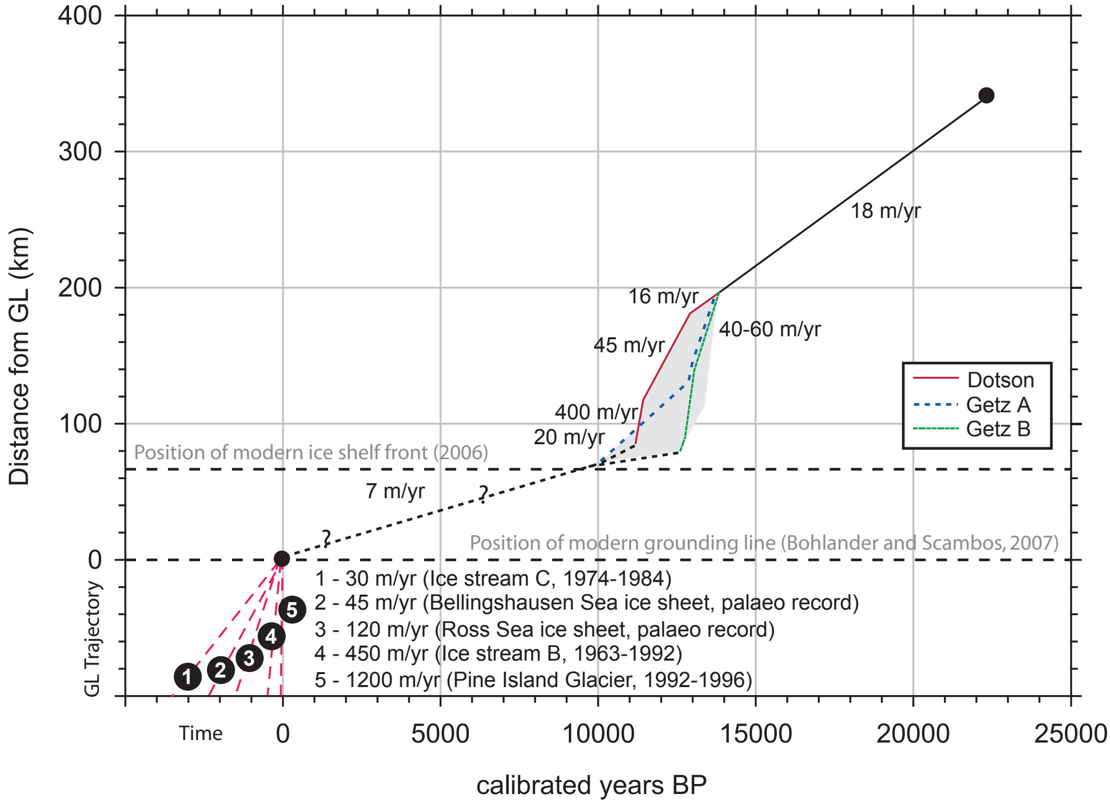

Figure 8

Figure8.

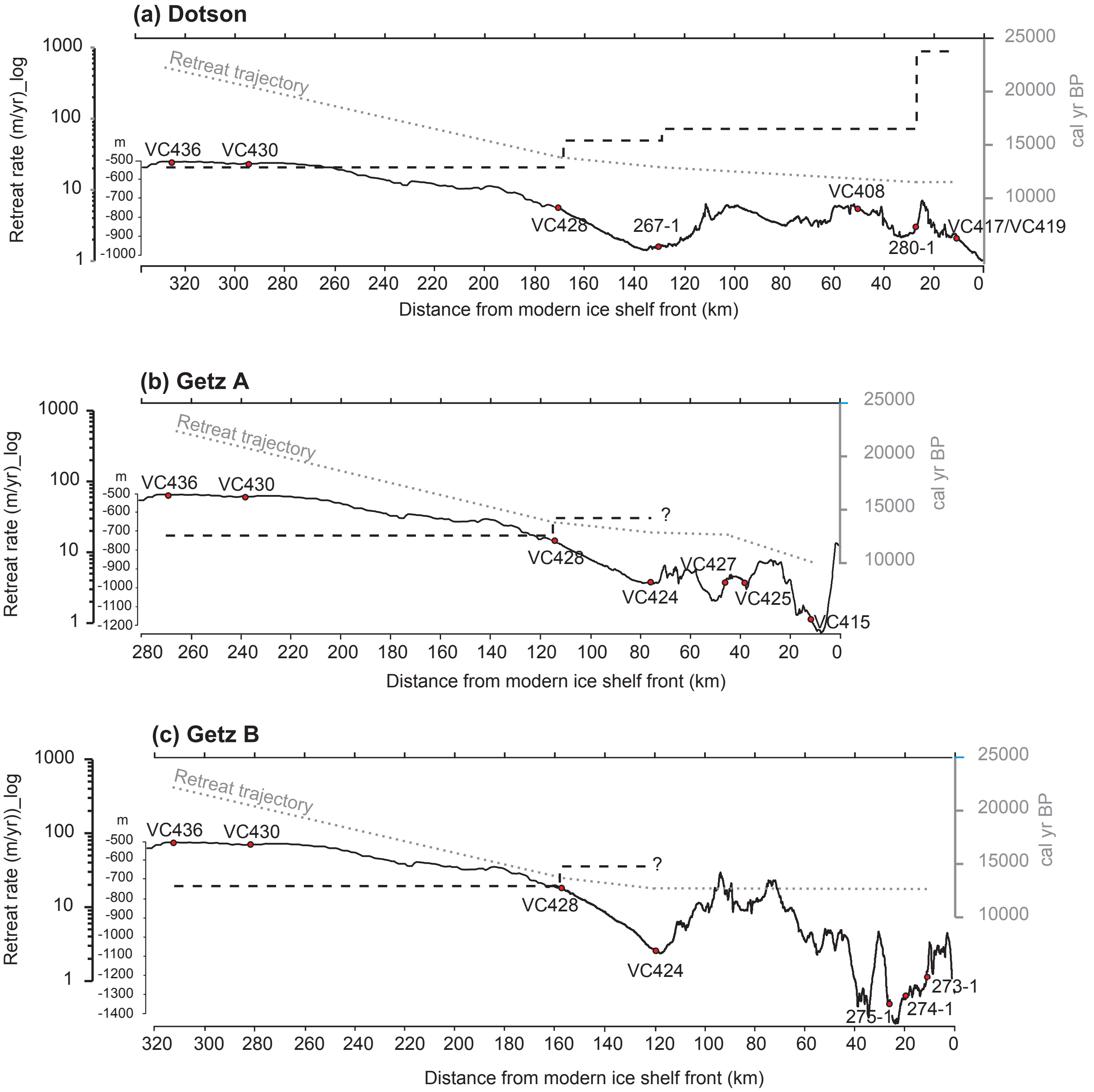

Supplementary Table 1.

Core		Parameter measured								
Gear	ID	MSCL	MS2F point sensor	Shear strength	Water content	Grain-size	TC	C_{org}	N_{tot}	Clay mineral
VC	VC408	✖		✖	✖	✖				✖
VC	VC411	✖		✖	✖	✖				✖
VC	VC415	✖		✖	✖	✖	✖	✖	✖	✖
VC	VC417	✖		✖	✖	✖	✖	✖	✖	✖
VC	VC419		✖	✖	✖	✖				✖
VC	VC422	✖		✖	✖	✖	✖	✖	✖	✖
VC	VC424	✖	✖	✖	✖	✖	✖	✖	✖	✖
VC	VC425			✖	✖	✖				✖
VC	VC427	✖		✖	✖	✖				✖
VC	VC428	✖		✖	✖	✖	✖	✖	✖	✖
VC	VC430	✖		✖	✖	✖	✖	✖	✖	✖
VC	VC436	✖		✖	✖	✖	✖	✖	✖	✖
GC	PS69/259-1	✖		✖	✖	✖	✖	✖	✖	✖
GC	PS69/265-3	✖		✖	✖	✖	✖	✖	✖	✖
GC	PS69/267-1	✖		✖	✖	✖	✖	✖	✖	✖
GC	PS69/273-2	✖	✖	✖	✖	✖	✖	✖	✖	✖
GC	PS69/274-1	✖	✖	✖	✖	✖	✖	✖	✖	✖
GC	PS69/275-1	✖	✖	✖	✖	✖	✖	✖	✖	✖
GC	PS69/280-1	✖		✖	✖	✖	✖	✖	✖	✖

Supplementary Figure 1a-d.

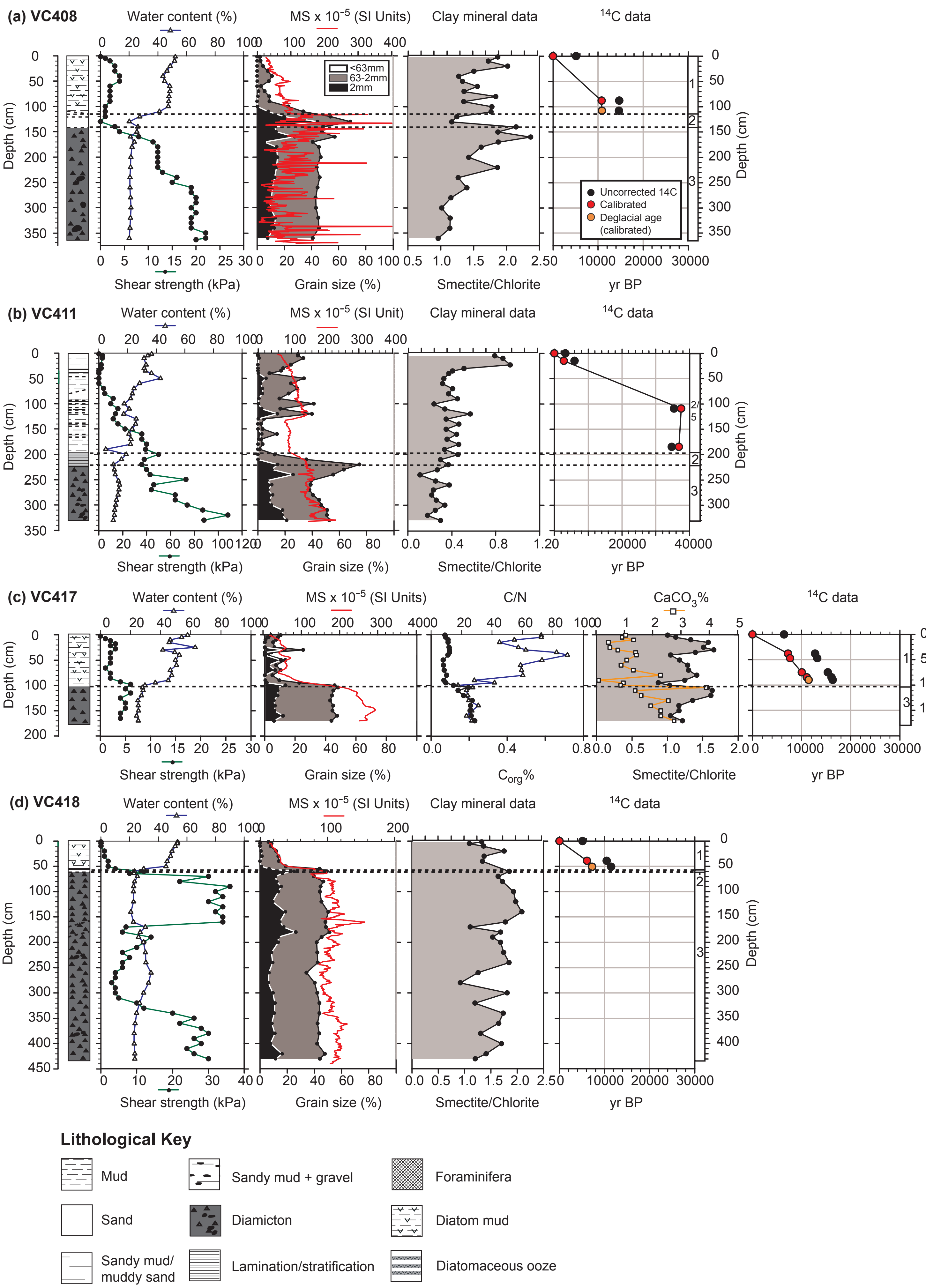

Supplementary Figure 1e-g.

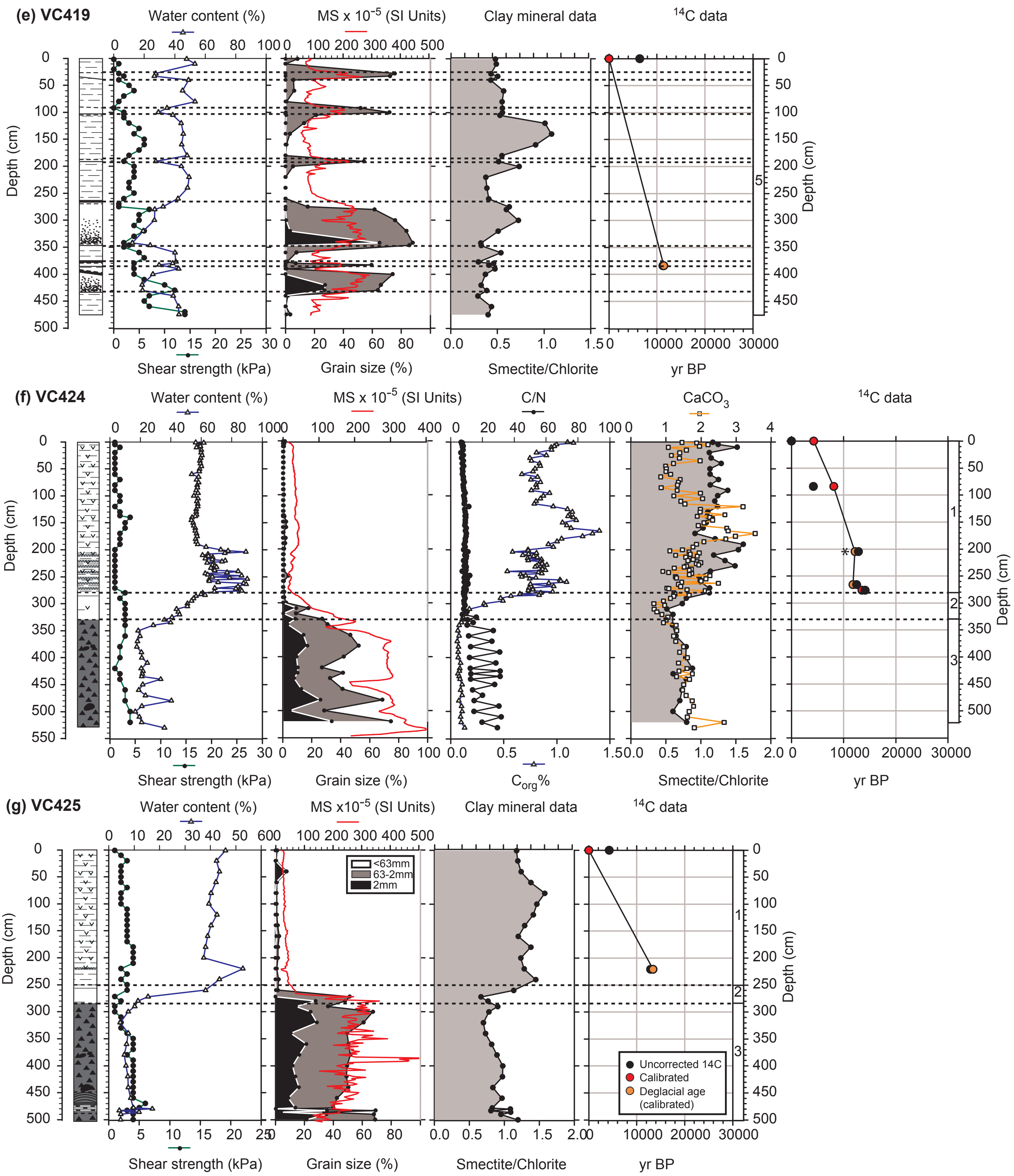

Supplementary Figure 1.h-j.

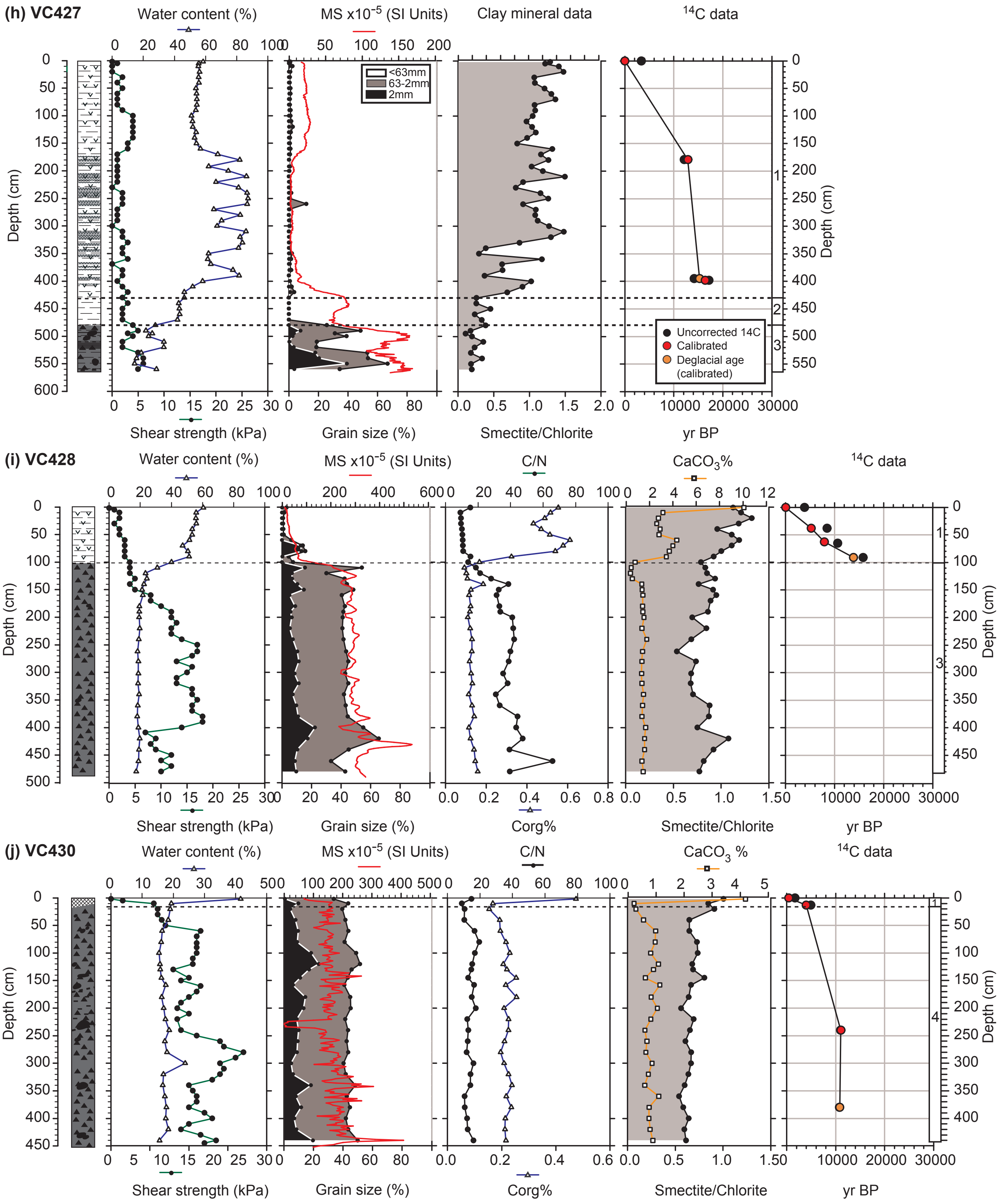

Supplementary Figure 1k-n.

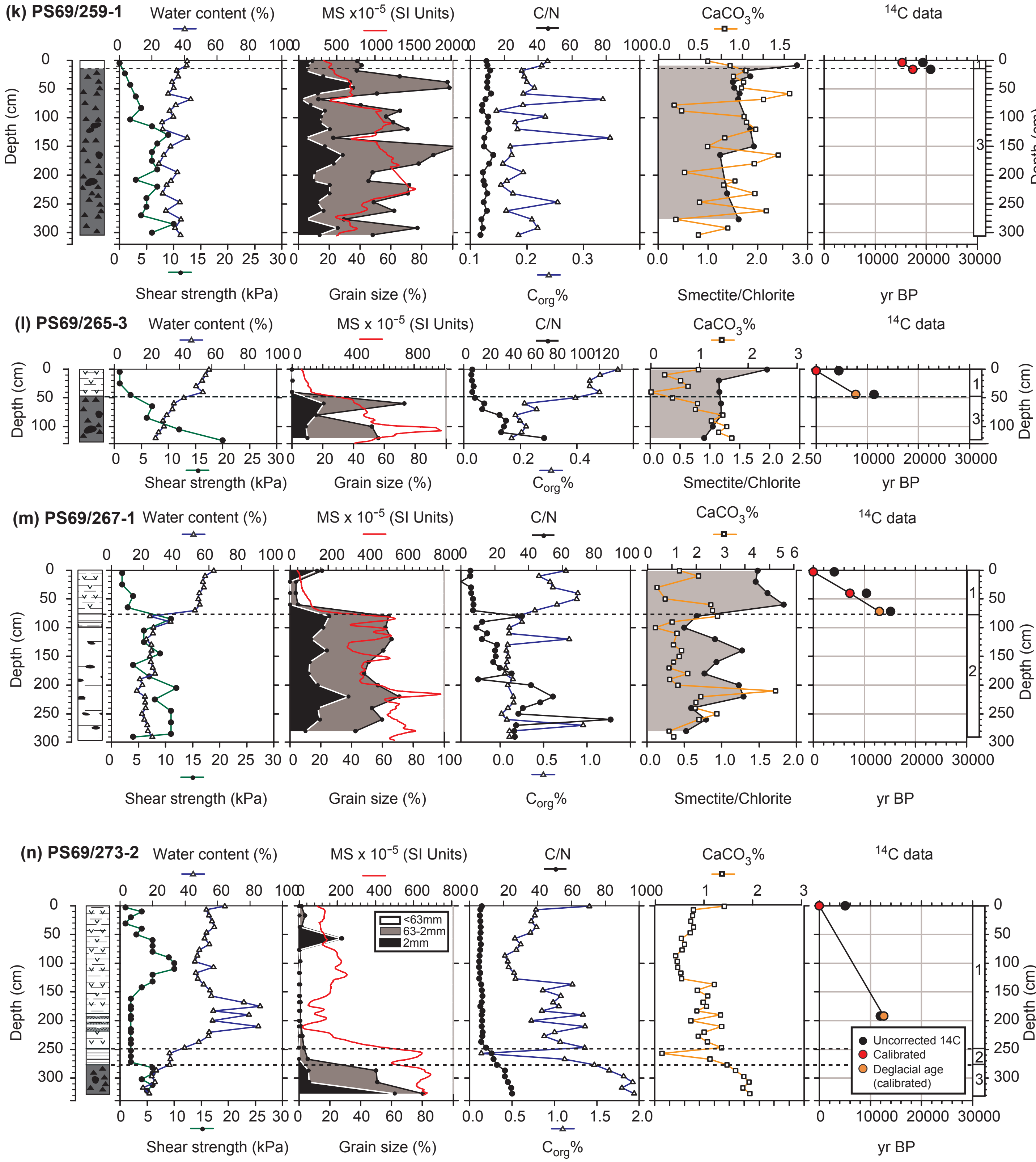

Supplementary Figure 1o-q.

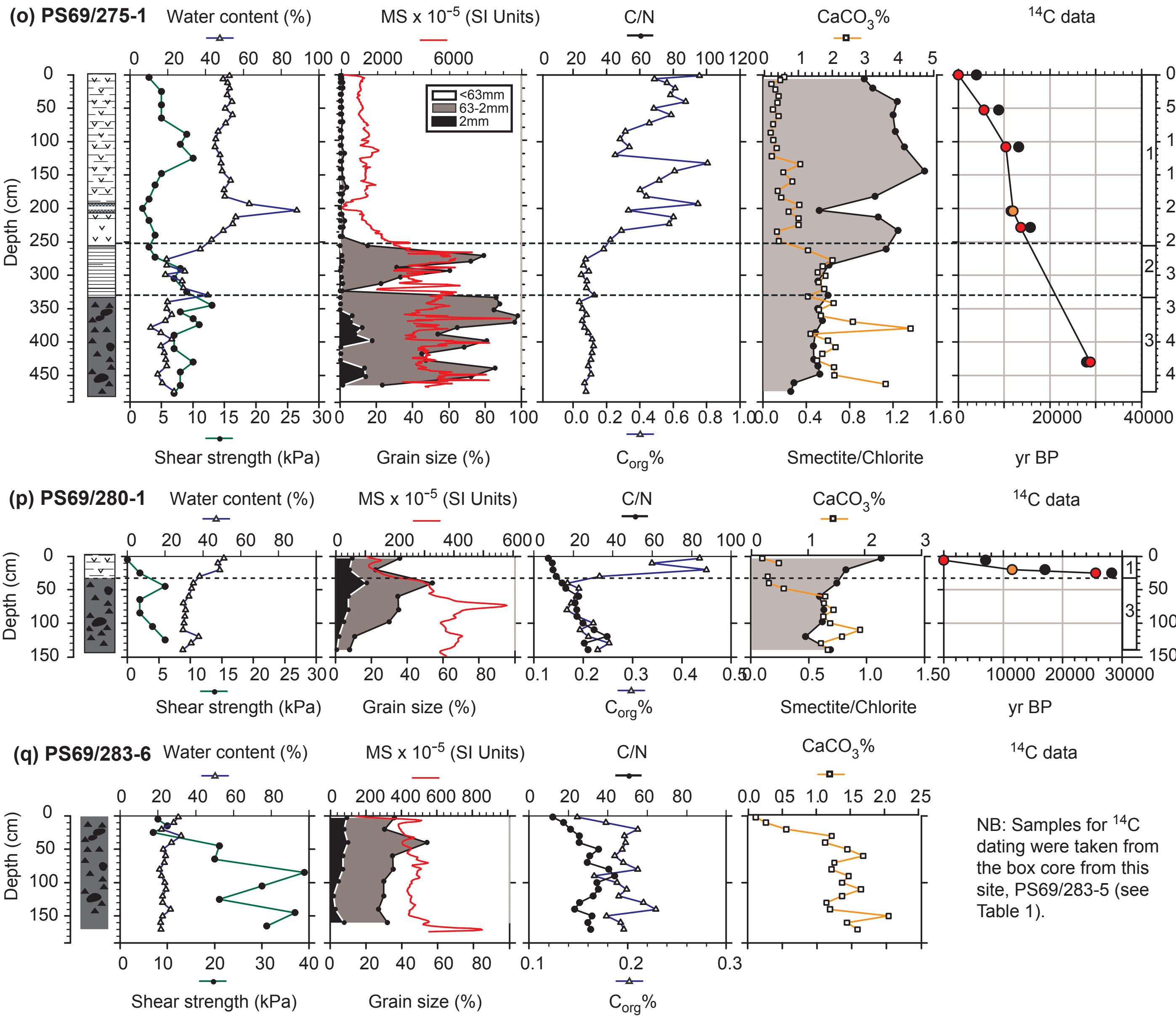

NB: Samples for ^{14}C dating were taken from the box core from this site, PS69/283-5 (see Table 1).